

UCLA

UCLA Electronic Theses and Dissertations

Title

Design and Validation of a Skin-Covered, Linkage-Driven Implantable Prosthesis

Permalink

<https://escholarship.org/uc/item/2nn1r2pg>

Author

Lai, Gracia Valerie

Publication Date

2022

Supplemental Material

<https://escholarship.org/uc/item/2nn1r2pg#supplemental>

Peer reviewed|Thesis/dissertation

UNIVERSITY OF CALIFORNIA

Los Angeles

Design and Validation
of a Skin-Covered,
Linkage-Driven Implantable Prosthesis

A thesis submitted in partial satisfaction
of the requirements for the degree of Master of Science
in Bioengineering

by

Gracia Valerie Lai

2022

© Copyright by
Gracia Valerie Lai
2022

ABSTRACT OF THE THESIS

Design and Validation
of a Skin-Covered,
Linkage-Driven Implantable Prosthesis

by

Gracia Valerie Lai

Master of Science in Bioengineering

University of California, Los Angeles, 2022

Professor Tyler R. Clites, Chair

The soft fur of an animal, the pain that protects us from the burn of a hot mug, and the tender touch of a loved one, are sensations we often take for granted. Unfortunately, people with hand prostheses have only the ability to hold and move objects but they cannot “feel” the object. Providing sensation through a prosthetic device is a major unmet need. Current prostheses lack the sensory feedback mechanism to take in data from external environments and convert it into “natural” sensation for the user. The objective of this study is to find a functional solution for people with thumb amputations that restores embodiment of the prosthesis and sensation to the thumb.

This thesis proposes a surgical and mechanical solution to transfer skin onto a novel implantable prosthetic thumb. Since current designs of prosthetic fingers do not allow for

fixation to the bone and implantation under the skin, the first aim of this study is to design a prosthetic thumb that is implantable, allows for osseointegration with the residual phalanx, and restores grasp motion. To test the surgical solutions, the second aim of this study is to design a rat model that utilizes similar surgical techniques and allows for implantation of a prosthesis.

The thesis of Gracia Valerie Lai is approved.

Justine C. Lee

Liang Gao

Nabil J. Tawil

Tyler R. Clites, Committee Chair

University of California, Los Angeles

2022

Table of Contents

Chapter 1: Motivation and Background	1
1.1 Introduction.....	1
1.2 Hand Anatomy, Biomechanics, & Amputation.....	2
1.3 Skin Flap Transfer	4
1.4 Flap Prefabrication and Prelamination	6
1.4.1 Prefabrication Process.....	6
1.4.2 Prelamination Process.....	7
1.4.3 Comparison of Prefabrication and Prelamination.....	8
1.5 Osseointegration.....	8
1.6 Targeted Skin Reinnervation.....	10
1.6.1 Nerve Anatomy, Damage and Regeneration	10
1.6.2 Cutaneous Nerve Regeneration.....	11
1.6.3 Methods to Evaluate Functional Nerve Recovery	12
1.7 Sensory Feedback of Hand Prostheses.....	13
1.8 Discussion.....	14
Chapter 2: Human Model.....	16
2.1 Introduction.....	16
2.2 Surgical Solution Design.....	18
2.3 Prosthetic Thumb Implant Design	21
2.3.1 Design Methodology Overview	21
2.3.2 Linkage-Driven Mechanism	22
2.3.3 Articulating Hinge Thumb Design.....	23
2.3.4 Compliant Mechanism Thumb Design	26
2.4 Abaqus FEA Simulation Results	29
2.5 Implant in Cadaver.....	34

2.6	Conclusion	37
Chapter 3: Rat Model		38
3.1	Introduction.....	38
3.2	Specific Aims	39
3.3	The Epigastric Flap.....	39
3.4	Materials and Methods.....	40
3.4.1	Flap Elevation and Rotation Surgery	40
3.4.2	Flap Motion Analysis.....	42
3.5	Results and Discussion.....	43
3.5.1	Flap Elevation and Rotation Surgery	43
3.5.2	Flap Motion Analysis.....	52
3.6	Rat Implant Design	53
3.7	Conclusion	56
Appendices.....		57
Bibliography		58

List of Figures

Figure 1: Motion of 4-bar linkage mechanism design. A: Finger extended. B: Finger flexed.

Arrow in image A indicates initiation of linkage motion. 22

Figure 2: Labeled linkage mechanism with fixation points and joints. 23

Figure 3: Articulating hinge thumb design fixated into residual proximal phalanx and metacarpal bone. The extended total length of the implant is 63.77mm, with a 14mm diameter, and 31.8mm from the proximal phalanx to thumb tip. 24

Figure 4: CAD drawing showing 60° ROM of thumb tip when MCP joint rotates to 75°..... 25

Figure 5: Perspective images of the thumb implant showing hinge design..... 25

Figure 6: Notch flexure design. A: Perspective view. B: Side view..... 26

Figure 7: Compliant Thumb Design with cruciform for IP joint. A: Front view B: Side profile. C: Back view. The length of the whole implant is 70.5mm. The length from the proximal phalanx to thumb tip is 32.5mm. The diameter of the implant is 14.56mm diameter. The cruciform is 5mm wide, 20.34mm in length, and 0.4mm thick. The flat compliant below the cruciform is 10.15mm in length, 3mm wide, and 0.3mm thick. The flat compliant rotating parallel to the MCP is 16mm length, 1mm wide, and 0.3mm thick. 27

Figure 8: Cross-pivot thumb design. A: Front view B: Top profile. C: Back view..... 28

Figure 9: Coverage design of cruciform IP joint. 29

Figure 10: Boundary conditions and load for Abaqus simulations..... 30

Figure 11: Before and after deformation of flexure. Implant design with 0.5mm cruciform thickness and 0.3mm bottom flat flexure thickness with LDPE. At yield stress, range of motion is 50°. The red dots and line indicate the angle that was measured for range of motion. 30

Figure 12: Implant design with 0.6mm cruciform thickness and 0.3mm bottom flat flexure with LDPE. At yield stress, range of motion is 40°	31
Figure 13: ROM at Yield Stress for LDPE and HDPE of 0.4, 0.5, and 0.6mm cruciform thicknesses.	31
Figure 14: Stress and ROM at hard stop of 0.4, 0.5, and 0.6mm cruciform thicknesses.....	32
Figure 15: FEA results of cross pivot design. Max stress: 8.48 MPa.	33
Figure 16: Loaded results of cross pivot design.	34
Figure 17: A: Flexor pollicis brevis muscle, A1 pulley tendon, palmar digital nerves. B: Amputated proximal phalanx.....	35
Figure 18: Arrows showing implant fixation and insertion points.	35
Figure 19: Opposition motion of the implant, right image shows implant under the skin.	36
Figure 20: Thumb in extension, right image shows extension of implant under the skin.	36
Figure 21: Thumb in flexion, right image shows flexion of implant under the skin.	36
Figure 22: ‘Tennis racket’ shape flap drawn in the epigastric region.....	41
Figure 23: Images of epigastric vessel from dissection of rat cadavers.....	41
Figure 24: Bottom, center, and top points tracked on the rotated flap.....	43
Figure 25: Changes of flap strain as hind leg rotates and stretches over 4 cycles. Blue line shows the strain between bottom and center points (proximal strain). Black line shows the strain between center and top points (distal strain).....	52
Figure 26: Implants part 1 and 2 manufactured by Anatomics Starpore material (porous HDPE).	55

Figure 27: A: Implants inserted in the ‘tubularized’ rotated flap. B: Closed ‘tubularized’ flap with implant when hind leg is extended. C: Closed ‘tubularized’ flap with implant when hind leg is flexed. 56

List of Tables

Table 1: Human cadaver dissection images for index finger prosthesis implantation procedure. 19

Table 2: Images of control group 1 rats with flap elevation, from Day 1 to Day 10+ post-op..... 44

Table 3: Images of rotation flap model 1 vs. rotation flap model 2..... 45

Table 4: Images of rotation model 2 vs. rotation model 3. 46

Table 5: Images of Rotation model 3..... 49

Table 6: Design iterations of rat implant. 53

Acknowledgements

First and foremost, I would like to thank my advisor, Professor Tyler Clites, for introducing me to the field of implantable prosthetic devices and giving me the opportunity to kick off and take ownership of this project. Tyler, it has been a privilege working under your guidance and in your lab. Our collaboration did start in the middle of a pandemic while I was halfway across the world, but in my time here I was able to grow so much as a student and researcher and gain confidence in my research, writing, communication, and presentation skills. Your passion, drive, and excitement for research and mentorship is truly inspiring and very special. Thank you for always giving me constructive criticism, challenging me to work out of my comfort zone, being so patient and understanding, and providing me with the support that I need.

I would also like to thank everyone in our surgical team: Dr. Kodi Azari, Dr. Lauren Wessel, Dr. Nirbhay Jain, and Dr. Meaghan Barr. The surgical solution to this project and animal work would not have been possible without you all. I really appreciate getting to work alongside and learn from each of you. Thank you for taking time out of your very busy schedules to collaborate and provide insight on this project.

Everyone in the Anatomical Engineering Group, thank you for creating a home away from home. Ophelie, I am so grateful for our friendship, and I cannot thank you enough for your support. Brandon, thank you for your willingness to pass on your knowledge and answering the many questions that I had. Will, you are always willing to jump in and the first to offer help. Carlos, I will miss our evening lab talks, always appreciate the life advice you give me. Alex, thank you for the career advice and guidance in research work. Alyssa, Solidworks is so much easier when you are around. Marcus, I appreciate your enthusiasm and work that you have put

into this project. Andy, thank you for carrying on this project, can't wait to see what you will accomplish.

Finally, I would like to thank my parents for the immense support and freedom they have given me to explore my passion, study abroad, and grow independently. It has not been easy being so far from you both, but I would not have gotten to this point in my life without your encouragements and confidence that you have in me.

Chapter 1: Motivation and Background

1.1 Introduction

Limb amputation typically causes a loss of function that can interfere with activities of daily living. There are approximately two million people in the United States with limb loss, most of them caused by vascular disease and trauma (Limb Loss Statistics n.d.). Among the traumatic amputations, 78% of the cases involve upper extremities, and 90% of those involve partial hand amputations (Ilario Imbinto et al. 2016). Although prosthetic devices have greatly advanced in the past decade to replace the function of the amputated limb, hand prosthetic devices remain limited due to the confined space and complexity of the human hand.

The hand is an exceptionally versatile part of the body and has enabled humans to evolve as functional and creative beings. Most everyday activities require the grasp of an object, promoted through the opposition motion of our thumb. Losing the thumb alone causes loss in 40% of the overall hand function (Moran & Berger, 2003). Additionally, finger amputation cuts off cutaneous sensations that are provided through a dense and complex sensory receptor system in our fingertips. Current commercial finger prosthetic devices are unable to communicate neural sensation (touch/proprioception) to the human nervous system and cannot integrate with the skeletal system. Without these abilities, the user lacks sensation and embodiment of the prosthesis.

To address these shortcomings, this thesis proposes the combination of surgical and mechanical solutions to transfer sensate skin onto an implantable prosthetic device. By utilizing natural human skin, the user benefits from innate biological sensory receptors that allow them to feel what the prosthesis is “feeling”. Existing techniques such as prelamination (Chiang, 2006),

skin flap transfer (Parrett & Pribaz, 2010), and reinnervation (Kostakoğlu et al., 1994) are integrated into the surgical solution. To replace the function, movement, and shape of the thumb, I am proposing a new design of an implantable prosthesis that restores joint motion and directly integrates into the bone.

1.2 Hand Anatomy, Biomechanics, & Amputation

When designing a prosthetic finger, it is important to consider and understand the components of each finger that should be included in the prosthesis design to restore essential functions. Each finger consists of three miniature long bones (“phalanges”), including the distal, middle, and proximal phalanx. These bones are connected by 3 joints: the metacarpophalangeal joint (MCP, also known as the knuckle joint), proximal interphalangeal joint (PIP, between the bottom and middle phalanges), and distal interphalangeal joint (DIP, between the middle and distal phalanges). To perform finger flexion, there are two extrinsic muscles, flexor digitorum profundus and flexor digitorum superficialis (Bajaj et al. 2021). The thumb is unique as it has a similar bony anatomy, but no middle phalanx. The thumb’s phalanges are connected by the carpometacarpal (CMC) joints, which oversees flexion/extension, abduction/adduction, and opposition/reposition movements. The muscles involved at the carpometacarpal joints include flexor pollicis longus and flexor pollicis brevis. The two muscles that help flexion and extension of the IP joint are the flexor digitorum superficialis and flexor digitorum profundus. (Hand anatomy | HealthEngine Blog 2008)

Partial hand amputation is defined as amputation that does not affect wrist movement. There are 4 levels of partial hand amputations (Ilario Imbinto et al. 2016):

1. Transphalangeal (one or more fingers)
2. Thenar (involves thumb)
3. Transmetacarpal distal (across palm, with or without thumb)
4. Transmetacarpal proximal (near wrist, with or without thumb)

Partial or complete amputations are often recommended for mutilating hand injuries. This is because long-term stiffness and pain in a salvaged digit can inhibit the rehabilitation of the remaining hand. Immediate amputations happen when four out of six of the basic digital parts (bone, joint, skin, tendon, nerve, and vessel) are injured (Moran and Berger 2003). There are several considerations when performing amputations, most importantly, how digital loss impacts overall hand function. For example, the thumb would be the top priority to be salvaged as it provides 40% to 50% of the overall hand's function (Moran and Berger 2003). The importance of the thumb lies with its positioning, allowing it to provide motors for opposition. If the thumb is injured, reconstructing the opposition, pinch, and abductor pollicis brevis (a muscle required for functional opposition) should be priority. A scar in the thumb remnant should be avoided as subterminal and precision pinch will be compromised if the scar is unstable or painful. Other than the thumb, a single digit amputation does not result in loss of essential hand function. When determining functional outcomes for digital amputations, the motivation of the patient is more important than the actual digits retained (Brown 1982).

In cases where multiple digits must be amputated, which is common in mutilated hand injuries, preservation of the thumb and a single digit alone will allow for grasp motion. Reconstruction of a third digit is recommended for optimal function. It is important to maintain

the thumb web space and adequate length of opposable ulnar post when reconstructing digits.
(Moran and Berger 2003)

1.3 Skin Flap Transfer

To reconstruct skin on a prosthetic finger, we can leverage existing techniques used in skin replantation. Current methodologies to promote skin healing or to replace the skin are chosen based on how severe and deep the wound is. The skin has three layers: the epidermis (outermost layer), dermis (contains connective tissue, hair follicles, and sweat glands), and deep subcutaneous tissue (hypodermis, made of fat and connective tissue) (The Skin: Human Anatomy n.d.). When the layers of skin are damaged, tissue engineering of the skin can be used as treatment. Engineered skin tissue is developed from either acellular materials or synthesized from autografts, allografts, xenografts, or synthetic sources to replace and aid healing of damaged skin layer(s) (Vig et al. 2017). Injuries at the epidermis can self-regenerate due to the presence of stem cells in that layer, while any deeper wounds larger than 4cm in diameter would need grafting as a treatment (Herndon et al. 1989). To this date, the technology to engineer a complete functional skin substitute is not available.

In cases with severe skin loss where tissue engineering solutions are inadequate, reconstructive plastic surgery techniques are used for skin replantation. A skin flap is a piece of skin removed from one part of the body to replace or repair damaged skin in another area. Degloving of the hand is an example of an injury that requires skin flap transfer. This is a severe injury where the top layers of the skin are separated from the muscle, connective tissue, and bone. Restoring skin on a partial degloved hand can be relatively straightforward, however, to

restore skin on an entire degloved hand would require multiple donor skin flaps, adding complexity to the surgery. For an injury where degloving of the entire hand occurs, three skin flaps are required to reconstruct the hand (Doctor et al. 2010). The goals of reconstruction in degloving cases can be summarized into 4 areas:

1. Prevent loss of function/ restore maximum function
2. Provide a stable hand with sensation
3. Prevent stiffness
4. Achieve good pinch and grasp motions

There are several flap options for hand re-surfacing used in plastic surgery. These include free flaps, which are tissue without vascular attachment. Examples include anterolateral thigh flap, radial forearm flap, lateral arm flap, scapular flap, etc. (Doctor et al. 2010). Skin flaps can be bulky, which will restrict movement and decrease the aesthetic of the hand. Flap defatting or thinning can be done where parts of the flap are excised. The radial forearm is a popular area to obtain the flap as it is very thin, pliable, and can be used to cover the thumb and first webspace.

A degloving case occurring distal to the wrist of the dominant right hand, showed successful reconstruction results, in which the patient was able to lift objects and write legibly (Doctor et al. 2010). The flaps used in the case study included the radial forearm flap that covered the first web space and thumb and the groin-hypogastric flap that covered the remnant fingers.

1.4 Flap Prefabrication and Prelamination

Flap prefabrication and prelamination are two methods that are used for skin reconstructive needs. Although they are not the primary methods for reconstructive needs, they are usually used for more sophisticated and complex situations. These methods are potentially helpful in our solution to minimize extrusion of the reconstructed skin flap over the thumb implant.

Flap prefabrication is when an axial blood supply is implanted into the donor tissue and is allowed to mature and neovascularize before being transferred to the recipient site. Flap prelamination is characterized by the implantation of tissues or devices in a vascular area prior to flap transfer (Pribaz, Fine, and Orgill 1999).

1.4.1 Prefabrication Process

To begin the prefabrication process, the requirements of reconstruction and available donor sites must first be defined. The color and texture of the donor site should match with the recipient site. This prefabrication process takes around 8 weeks and involves two stages. The first stage is where a vascular pedicle, which includes the artery and venae surrounded by adventitial tissue is dissected out and transferred to the desired area of tissue. The surrounding tissue of the implanted pedicle will spontaneously connect to the pedicle. Tissue expansion starts around week 1, where a tissue expander is implanted under the desired flap. The second stage is the transfer of flap after 8 weeks of maturation. A conservative 2:1 ratio (length of flap vs. extent of pedicle length within flap) is used to estimate the size of the flap in clinical cases. (Parrett and Pribaz 2010)

The outcome of prefabrication process reported in literature have been positive and mostly involve reconstruction of the face and neck areas for burn victims. Examples include

clinical cases of two patients suffering from extensive burns that underwent prefabrication process in the face and neck area. Results of these clinical cases showed successful transfer and healing of the skin (Parrett and Pribaz 2010).

1.4.2 Prelamination Process

The prelamination process also involves two stages. The first stage is where the graft material is introduced into the flap. A tissue expander may be used if needed. The location of the radial artery is a common territory used for prelamination. The second stage is flap transfer which occurs after a period of 3-4 weeks. (Parrett and Pribaz 2010)

Results of prelamination found in literature are also mostly positive. Examples of clinical case studies involving prelamination with different materials and in various parts of the body are summarized below:

- a. A clinical case of a patient with facial burns who underwent the prelamination process resulted in successful reconstruction of the nose, cheek and upper lip (Parrett and Pribaz 2010).
- b. Major ear reconstruction for patient with a birth defect was successfully constructed using tissue expansion, costal cartilage framework prelamination at the forearm, and microsurgical transfer (Chiang 2006).
- c. Osteofasciocutaneous fibular flaps were used for reconstruction of the neophallus in female-to-male transsexuals. This process offered many advantages including wide cortical bone for long-term intrinsic rigidity without the need for a penile prosthesis (Papadopulos, Schaff, and Biemer 2008). Prelamination technique with insertion of

penile prosthesis is also a common method, however, full functional use of the phallus after this method is low (Babaei et al. 2010).

- d. In this study, a titanium plate and anterolateral thigh prelaminated free flap was used in morphological reconstruction of the face. The metallic prosthesis was implanted in the left thigh at the suprafascial level. After 3 months, the prosthesis was covered by well-vascularized soft tissue (Crainiceanu et al. 2016).

1.4.3 Comparison of Prefabrication and Prelamination

A study was conducted to compare prefabrication and prelamination on 32 patients needing intraoral reconstruction after radical oncological surgery. Results showed that prelaminated fasciomucosal flaps experienced a higher shrinkage rate and early wound healing difficulties in comparison to fasciocutaneous non-prelaminated flaps. Donor site problems occurred more frequently in non-prelaminated cases (Poeschl et al. 2003). In order to reduce donor site morbidity, epifascial dissection (Webster and Robinson 1995) or de-epithelialization methods can be used to harvest the flap (Kawashima et al. 1989).

1.5 Osseointegration

Our solution includes fixating the thumb implant into the residual proximal phalanx, allowing the user benefits from embodiment and stability of the prosthesis through osseointegration. Osseointegration is defined as the direct attachment of an implant to a bony residuum by the formation of bony tissue around the implant without the growth of fibrous tissue at the bone-implant interface (Manurangsee et al. 2000). During the 1950s, it was found that

chambers made with titanium can be incorporated with bone tissue (Branemark 1983). This phenomenon occurs due to bone fusing with the titanium oxide layer, which allows a stable integration that can only be separated by fracture. It is hypothesized that a unique hydrated epoxy matrix forms between the titanium implant and the living tissue. This is unique to titanium as other metals lack the solubility or stability to form such a complex matrix (Brånemark et al. 2001). Additionally, Patients with osseointegration of the implant experience a phenomenon called osseoperception, where they are able to identify tactile thresholds transmitted through their prostheses (Brånemark et al. 2001). The osseointegrated fixture allowed for both return of mechanical and sensory functionalities.

This method is very common among dental prostheses as well as bone-conducting hearing aids. Osseointegration used on a finger prosthesis involves the insertion of a threaded titanium implant in the medullar canal of the bone structure and locking the prosthesis in place using a small transverse screw device (Jan de Cubber 2007). For the patient to have adequate function of the prosthesis, they must have a movable metacarpophalangeal (MCP) joint. This is a very simple procedure requiring only 30 minutes for the first stage and 10 minutes for the second stage (Manurangsee et al. 2000).

Three case studies (Manurangsee et al. 2000) conducted in Thailand, found that this technique allowed for a stable prosthesis fixation, transfer of motor function, and perception of sensation. The same study demonstrated that grip strength increased in the hand with an osseointegrated prosthesis compared to a normal hand. This was because sensation was transmitted from the hard acrylic prosthesis to the bone, which allowed the patient to transfer power back to the prosthesis. Results showed that the patients were able to perform daily activities, but they took longer to do delicate activities like writing and picking up small objects.

On the other hand, they took a shorter amount of time to pick up large objects when compared to patients without prostheses. These results indicate that patients with prostheses had better gross movements but weaker fine movements. This is due to the missing sensation through the skin, an important factor in performing finer movements.

Patients that undergo osseointegration after limb amputation have improved prosthetic use, comfort, walking ability and quality of life. However, with osseointegration, there is always a risk of infection, most commonly low-grade soft tissue or superficial infections that are at the skin-implant interface (Kunutsor, Gillatt, and Blom 2018). Infections can be treated with antibiotics, but osteomyelitis can occur in severe cases, leading to further amputation or sepsis. Osseointegration solutions for finger prosthetic devices are unheard of in the U.S., potentially due to the high risk of infection at the exposed osseointegration site.

1.6 Targeted Skin Reinnervation

Reinnervation helps restore sensation in a skin flap, which is achieved through the connection of nerves in the skin flap with nerves at the recipient site. This is a useful technique that can be used in our solution to optimize the sensation in the flap after it has been transferred onto the prosthetic thumb.

1.6.1 Nerve Anatomy, Damage and Regeneration

Reinnervation is quite effective because the neurons in the peripheral nervous system, unlike the central nervous system, can regenerate due to the fast cleanup of damaged cells and assistance of Schwann cells. Regeneration can occur at a rate of 1mm/day as long as the soma is

not damaged. (Peripheral Neurological Recovery and Regeneration | PM&R KnowledgeNow n.d.)

When an injury that separates the proximal and distal ends of the nerve occurs, the distal end of the nerve undergoes Wallerian degeneration, in which the distal end of the nerve dies. After the degeneration of the distal nerve ending, neuronal regeneration occurs at the proximal end of the injury.

Neurotmesis is the most severe injury of the nerve and occurs during amputations. The return of functionality depends on the severity of neurotmesis:

- a. Endoneurium → fair growth
- b. Perineurium → poor growth
- c. Epineurium → no growth

1.6.2 Cutaneous Nerve Regeneration

There are 2 different modes of cutaneous sensory reinnervation: the regenerative growth of injured nerve, and the collateral sprouting of neighboring intact nerves. In traumatic or surgical nerve injuries of the hand, partial recovery of sensations are observed long before nerve regeneration can occur (Inbal et al. 1987). This finding contributed to the conclusion that recovery of sensory functions is due to collateral sprouting, in which innervated and denervated tissues adjoin, in the absence of nerve regeneration (Rajan et al. 2003).

In a study (Rajan et al. 2003) on epidermal reinnervation, two models of intracutaneous axotomy were compared. The first model was the “incision” model, where 3mm diameter and 3-4mm deep circular incisions were made on the back of each subject. The second was the “excision” model, where incisions of the same dimensions were made followed by removal of

the incised tissue which included the epidermis and dermis. After some premediated months (varying for different samples), they made the same excisions, took them as biopsies and analyzed patterns of axonal regrowth using standard and confocal fluorescence microscopy. Results showed that in the incision model, complete denervation and Wallerian degeneration were achieved in all subjects. In both models, there were axonal regeneration of the epidermal axons just outside the incision lines. However, regenerative axonal regrowth in the dermal axons was minimal and collateral sprouting was dominant in the excision model subjects.

A case study involving people with arm amputations (Kuiken et al. 2007), demonstrated the development of a technique designed to transfer remaining arm nerves to the residual chest muscles. The sensory nerve fibers were able to regenerate through the muscle to the skin. Within 5 months, patients developed touch sensations on their chest that was perceived to occur on their amputated arm. One patient even felt sensations of joint position, skin stretch, edge sensation, and a strong proprioceptive feeling of their fourth finger being extended. The study mapped out different parts of the chest that correlated to sensations in different parts of the arm and hand. In addition, they tested for sensory and pain thresholds using surface electrical stimulation. At ranges of 2.0 mA to 5.0 mA, non-painful sensations were observed. Painful sensations were observed from 11.0mA to 36.0mA. It was suggested that since reinnervation surgery happened more than a year after the patient's amputation, peripheral and central sensory pathways can remain viable even after prolonged periods of dormancy.

1.6.3 Methods to Evaluate Functional Nerve Recovery

Analyzation methods used to study nerve regeneration include histomorphometry analysis, immunostaining, and confocal microscopy of axons (Rajan et al., 2003) (Brenner et al.

2006). However, functional aspects of nerve recovery are poorly correlated to the data shown in electrophysiological and histomorphometrically analysis (Dijkstra et al. 2000). In addition, most methods for evaluating sensory nerve recovery are invasive and not applicable to longitudinal studies (Zeng et al. n.d.).

Withdrawal response is a useful way to test for sensory nerve recovery, in which the two copper wires of a bipolar electrode are placed 3mm apart to stimulate the foot sole in an adult rat (Dijkstra et al. 2000). The normal reaction of a rat to stimulation (0.1 mA) would be withdrawal of its foot and spread of its toes. In the first few weeks after reinnervation surgery, there was no reaction from the rats. However, some of the rats evoked a withdrawal reflex at high stimulation intensities after 3 weeks, and at 21 weeks post-op a withdrawal reflex was seen in 90% of the rats at 0.33mA.

1.7 Sensory Feedback of Hand Prostheses

Patients with a prosthetic hand have only visual knowledge that they are holding an object but cannot feel the shape and stiffness of the object. An ideal prosthetic hand would allow a bidirectional link between the user's nervous system and the environment surrounding the hand. To do so, the remaining central and peripheral neural networks in sensory feedback and motor control would have to be integrated with the prosthetic device (Raspopovic et al. 2014).

There are several types of hand prostheses: passive prostheses, body-powered prostheses, and battery-powered prostheses. With body-powered prostheses, the forces developed from the body are mechanically transmitted to a terminal device. Kinesthetic and proprioceptive feedback are transmitted to the patient through a control cable. The control of the prosthesis originates

from the shoulder, wrist, or finger. Depending on the origin, the source of power varies. Battery-powered prostheses are used for patients that have severe scar tissue, cannot generate sufficient force, or do not have a wide range of motion. These prostheses are activated by the user's input signals from the residual limb and are electrically processed to control the device (Ilario Imbinto et al. 2016).

In a case study (Raspopovic et al. 2014) of a participant with a transradial amputation, sensory feedback and real-time closed-loop control of the prosthetic hand by the patient was shown to be successful by stimulating peripheral nerve fascicles. In addition to that, they were able to restore touch sensation by connecting transversal interfascicular multichannel electrodes (TIMEs) to the prosthetic hand sensors and implanting them in the median and ulnar nerve fascicle. The motions of the hand were controlled by the remaining muscles on the residuum of the amputated hand. Several trials were completed to confirm that the restored touch sensation allowed for high performance control of the prosthesis.

1.8 Discussion

Although partial hand amputation is globally the most common amputation level due to traumatic injuries (Ilario Imbinto et al. 2016), its available treatments have not progressed far. There are several limitations for restoring the hand after amputation which include the diversity in range of movements, the complexity of function and anatomy of the hand, and the size of technology needed. Additionally, full restoration of the hand may not be necessary as partial hand restoration can be functionally satisfactory as long as the opposition motion is restored (Ilario Imbinto et al. 2016).

Replantation of the injured hand would be the ideal treatment but, in some cases, the only solution is to fit a partial hand prosthesis. Prosthetic devices can be disconcerting visually and functionally for the patient. In addition, recreating sensation and connection between the prosthesis and surrounding environment remains an unresolved challenge.

The technique needed to reconstruct skin on a finger prosthesis can be best compared with ear reconstruction or total penile reconstruction for transgender patients. In those two cases, bones are usually harvested from the patient as opposed to using foreign material as graft. Similar surgical techniques can be used for our application, but experiments should be conducted to study the reaction of skin to a moving prosthetic device made of foreign material.

Chapter 2: Human Model

2.1 Introduction

The future vision of skin covered prosthetic devices creates the illusion of naturally reconstructed sensate limbs. To narrow down a specific prosthetic application, this thesis will focus on finding a solution for people with thumb defects. This includes people with aplasia, hypoplasia, and more commonly thumb amputations.

Thumb amputation is an ideal starting case for this work due to its dramatic impact on function, as well as the relative simplicity of the distal thumb joint. Many activities of daily living require opposition grasp, which is only possible with an independent, actuated thumb; loss of the thumb can reduce overall hand function by as much as 40% (Capek, Hughes, and Warden 2018). Amputation of the thumb not only causes challenges in power grip and precision motions, but also limits sensation due to the damage of highly concentrated sensory receptors in the thumb tip. A loss in sensations means a loss in environmental cues, physical connection, and protection from physical damage. Although losing a finger may sound trivial compared to a whole limb loss, our hands are involved in almost all activities of daily living and are always exposed and seen by others. Additionally, the traumatic amputation of the thumb brings about immense psychological impact. Losing a finger is more than a functional loss but also a loss of our self-image and representation to others.

Current solutions for thumb amputations can be summarized into passive, body-powered, and electrically-powered categories. These solutions have not advanced much over the years in terms of options and functionality. Designing a mechanism that can create diverse and intricate motions is quite challenging due to the confined space in the hand. The most used prosthesis for

people with thumb amputations are passive and are attached to the skin by suction or special adhesives. They can be removed easily, which restricts embodiment and connect between the prosthesis and the user. Additionally, they can cause skin irritation and do not provide any sensation to the patient nor restore joint motion. As such, patients with thumb amputations do not typically use a thumb prosthesis on a daily basis.

In addition to prosthetic solutions, there are existing surgical solutions that reconstruct the thumb for people with amputations at the metacarpal joint level. The Gilles cocked hat flip surgery takes the iliac crest bone graft and lengthens the thumb by 2cm (Manktelow 1986). This surgery does not restore joint function and limits the extension of thumb length. Another option is the toe-to-hand transfer procedure (Manktelow 1986). This allows for the restoration of the IP joint, sensation, and is aesthetically acceptable. However, the donor site morbidity is significant as a toe must be amputated.

To address the unmet needs of current solutions, we propose an implantable prosthesis that is anchored to bone and covered by native skin. Implanting a prosthetic device beneath the skin would allow for direct skeletal attachment, providing mechanical and sensory functionalities from osseointegration without the high risk of infection. Skin replacements are acquired from locations in the human body where skin is redundant and used as grafts or flaps to replace damaged skin (Doctor et al., 2010). These skin flaps can be transferred to the amputated site onto the prosthetic thumb. To provide motion and form to the skin, the design of the proposed implantable prosthesis would replace the function of bones, tendons, and shape of the thumb.

2.2 Surgical Solution Design




The surgical solution of the human model has been designed in consultation with our surgical collaborator, Dr. Kodi Azari, a practicing hand, microvascular, reconstructive plastic surgeon and professor of the Orthopedic Surgery and Plastic Surgery at UCLA. This human model will consist of the following plastic surgical techniques: prelamination, flap transfer, and reinnervation.



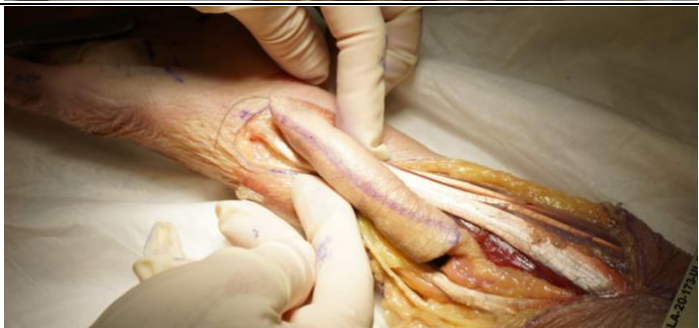


When implanting any foreign material in the body, there is always a concern that the implant can cause extrusion through the skin. Extrusion is when the surface of the implant protrudes the skin and is exposed. Incidences of extrusion are found with mandibular, breast, dental, and ocular implants. It is not entirely well known as to why this occurs, but it is hypothesized that extrusion is influenced by implant geometry, material, tissue ingrowth, foreign body response, and the amount of trauma in the skin tissue. To minimize the chances of extrusion, our human model will include a prelamination procedure of the thumb prosthesis in the donor site prior to skin flap transfer. This is where the prosthetic device is implanted under the donor flap for a period of six to eight weeks. The prelamination time should allow for the thumb implant to integrate with the skin without the interference of motion, minimizing disruption of soft tissue ingrowth. In addition, vascularization of the flap can be stabilized which reduces morbidity of the donor site (Fermi et al. 2021).

For our application, the radial forearm flap (RFF) is the most viable and appropriate choice as it can be used as a reversed radial forearm rotation flap. This means that the radial artery will be clipped on the proximal end of the flap and blood will be supplied through the distal end of the flap where the radial artery is left intact. After the flap is elevated, the prosthetic thumb is implanted. The flap is then ‘tubularized’ around the thumb before the incision is closed.

After six to eight weeks, a secondary surgical procedure will be conducted to rotate the ‘tubularized’ flap and implant onto the residual thumb. The prosthesis will be fixated into the medullary canal of the residual proximal phalanx and the metacarpal bone.

Table 1: Human cadaver dissection images for index finger prosthesis implantation procedure.

Procedure / Description	Hand Dissection Photos
Incision around radial forearm flap	
Antebrachial cutaneous nerve branch (can be included in the flap)	
Radial sensory nerve	

<p>Elevation of flap</p>	
<p>Early prototype of index finger prosthetic implant on elevated flap</p>	
<p>'Tubularized' flap around prosthetic device</p>	
<p>Linkage driven flexion motion of prosthetic device under skin flap</p>	
<p>Path of radial forearm flap to index finger</p>	

The procedure for thumb prosthesis implantation is similar to the procedure shown above. The difference between the procedure for thumb versus index finger is that the radial forearm flap cannot be used as a rotation flap for the index finger. Instead, it will be used as a free flap where the blood supply is clipped and the flap is completely isolated before transferring to the residual index finger. The blood supply will have to be anastomosed at the recipient site.

To provide native sensation in the flap, reinnervation procedure of the RFF flap will occur when the flap is transferred. This is where the lateral antebrachial cutaneous nerve (LACN) will be anastomosed in an “end to end” fashion with the digital nerve. Reinnervation will provide usable sensation in which the patient should be able to differentiate temperature, pressure, and pain for protection in their reconstructed thumb. However, the reconstructed thumb tip will still have a lower sensitivity degree than the natural thumb. To optimize the sensation in the finger, a FDMA flap (First Dorsal Metacarpal Artery Island Flap) or Littler flap transfer procedure can occur subsequently to the secondary procedure. This procedure is often used in thumb injuries, where the dorsal skin of the proximal phalanx of either the index or middle finger is transferred onto the thumb tip (Prabhu, Powar, and Sulhyan 2013).

2.3 Prosthetic Thumb Implant Design

2.3.1 Design Methodology Overview

This section describes the components, overall procedure, and design of the prosthetic thumb implant. This includes design constraints, computer-aided design (CAD) modeling with Solidworks, finite element analysis (FEA) simulation with Abaqus, prototyping, and cadaver work. The prosthetic thumb design proposed in this thesis is targeted for people with a functional MCP (metacarpal-phalangeal joint or the knuckle) joint, where the amputation occurs between

the IP (inter-phalangeal) and the MCP joints. Dimensions of the prosthetic thumb were determined from cadaver hand models, which were within the average dimensions of the metacarpal bone found in literature (Vaux et al. 2016).

The objective of the proposed thumb implant design is to restore opposition grasp motion in the hand. This requires a minimal range of motion (ROM), defined as the degree at which the thumb tip rotates. Literature provides the following values for thumb kinematics during opposition: ROM of $44.1^\circ \pm 19.7^\circ$ for the IP joint, and $41.6^\circ \pm 12.6^\circ$ for the MCP joint (Li and Tang 2007). In addition to a ROM constraint, the design must be compact enough to fit under the reconstructed flap. It should allow for osseointegration to the residual proximal phalanx, increasing stability and embodiment of the prosthesis. The material of the implant must be biocompatible and provide proper mechanical properties. Ideally, the material would be porous to allow for fibrous ingrowth and stabilization of the implant. However, the joints of the implant should remain non-porous to allow for rotation under the skin.

2.3.2 Linkage-Driven Mechanism

To provide opposition grasp, the motion of this implant will be initiated through a linkage-driven mechanism (Figure 1).

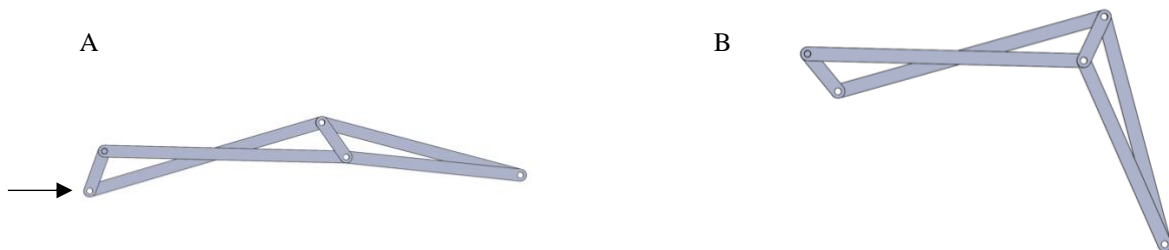


Figure 1: Motion of 4-bar linkage mechanism design. A: Finger extended. B: Finger flexed.

Arrow in image A indicates initiation of linkage motion.

This linkage mechanism architecture is well known and is often used in robotic hand designs (I. Imbinto et al. 2018). It consists of a 4-bar mechanism where the rotation of the MCP joint is coupled with the rotation of the IP joint. For our design, the implant is fixated to the hand in two areas, the metacarpal bone and the residual proximal phalanx (Figure 2). Due to the fixation sites of the device, rotation of the MCP joint causes linkage A to shift to the right, initiating the linkage-driven mechanism.

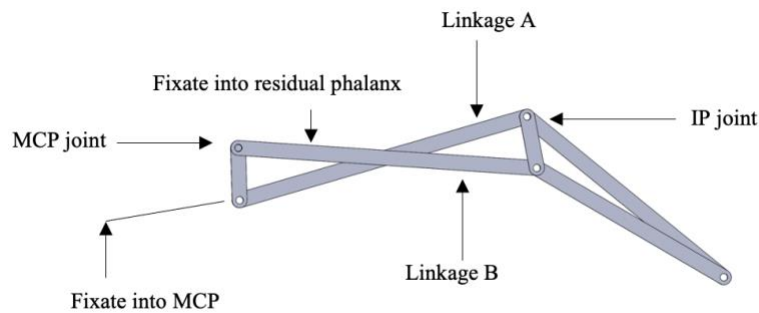


Figure 2: Labeled linkage mechanism with fixation points and joints.

2.3.3 Articulating Hinge Thumb Design

This design consists of 3 hinges, in which the IP hinge represents the IP joint and the MCP hinge rotates in parallel with the MCP joint. The proximal end of linkage A is screwed into the metacarpal and linkage B is fixated into the residual proximal phalanx. Linkage B is designed as a hollow cylindrical shape so that linkage A can cross through (Figure 3).

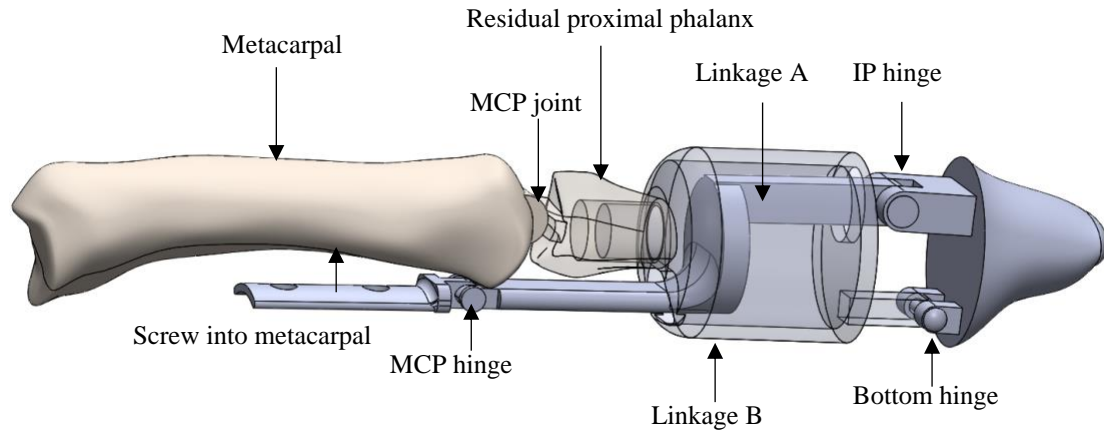


Figure 3: Articulating hinge thumb design fixated into residual proximal phalanx and metacarpal bone. The extended total length of the implant is 63.77mm, with a 14mm diameter, and 31.8mm from the proximal phalanx to thumb tip.

This design offers some flexibility in dimensions and ROM. The length and placement of each hinge affects how much the IP hinge rotates. As the mechanism is initiated, the IP hinge revolves around the bottom hinge while simultaneously rotating. The farther forward the IP hinge is set with respect to the bottom hinge when at rest, the larger the ROM. However, this will also cause linkage A to shift farther down as the MCP joint rotates. In this proposed design, the IP hinge is set slightly to the left of bottom hinge, allowing linkage A to stay within the bounds of linkage B as the mechanism is initiated. This design allows the MCP joint to rotate up to 75° before the MCP hinge hits the residual proximal phalanx, as shown in Figure 4. This ROM is more than sufficient to perform opposition grasp. As the MCP hinge rotates, linkage A is driven 7mm forward, allowing the IP hinge to rotate 60° .

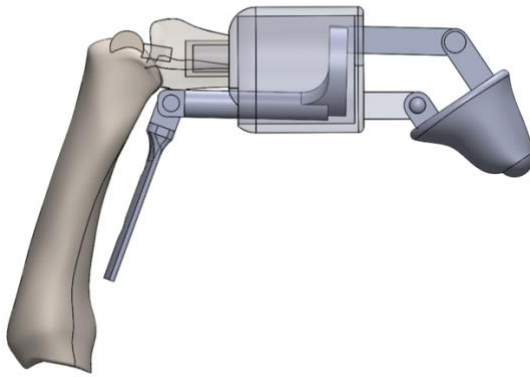


Figure 4: CAD drawing showing 60° ROM of thumb tip when MCP joint rotates to 75°.

The hinge design consists of metal (Ti6Al4V) articulation surfaces connected with a locking pin. Alternatively, part of the hinge can be made of polyethylene to create a metal-on-plastic articulating surface, reducing friction and wear.

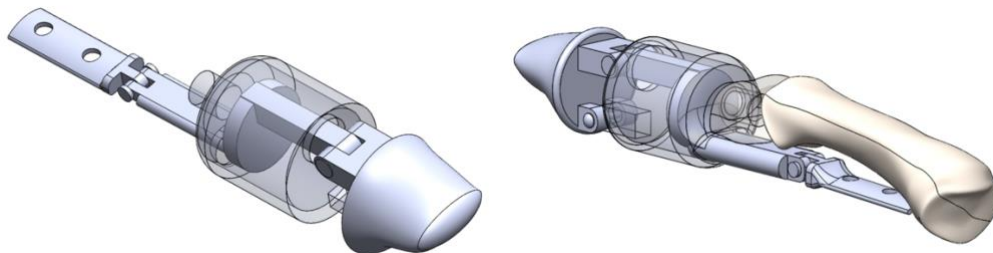


Figure 5: Perspective images of the thumb implant showing hinge design.

To shield the hinge mechanism motion from the skin, a dome-like coverage can be designed over the hinges. This would reduce changes of extrusion and retain thumb shape at the IP joint.

2.3.4 Compliant Mechanism Thumb Design

Compliant mechanisms offer an advantage over articulating surfaces because it decreases wear and minimizes aseptic loosening. Compliant mechanisms achieve motion via bending and deforming of the material rather than rubbing and sliding, allowing a longer part life. The angular deflection in a compliant mechanism is limited by material strength and geometric properties.

An alternate version of this design involves flexure hinges instead of rotational hinges. Except for the IP joint, the rotating joints are replaced with flat compliant mechanisms. The IP joint in the thumb design is reconstructed through a cruciform/ cross pivot/ notch mechanism. Therefore, the rotation and range of motion of the reconstructed IP joint is limited through the deflection of the flexure. Limiting factors of this design include the yield strength, Young's modulus, and Poisson ratio of the material. Other than material properties, the range of motion is determined by the thickness, length, height of flexure, and angle at which the blades cross.

Several types of compliant mechanisms were considered for the IP joint, including cruciform, cross pivot, notch, and flat compliant.

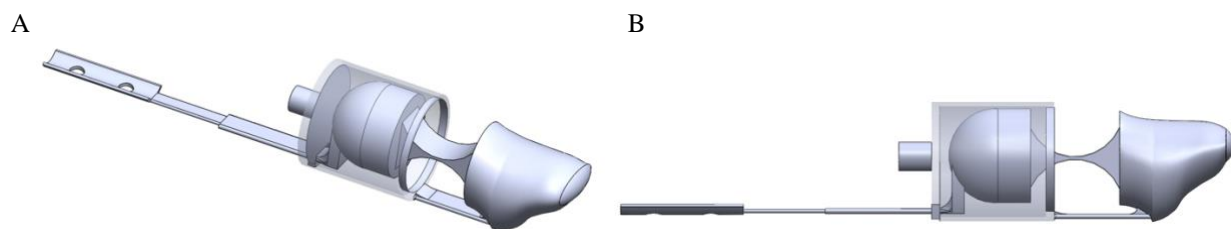


Figure 6: Notch flexure design. A: Perspective view. B: Side view.

The notch flexure design offered the most stability against torsion when under loaded conditions (Figure 6). However, the range of motion is lacking due to the high stress

concentration in the center of the notch. The cruciform design (Figure 7) offers a higher ROM when compared to the notch.

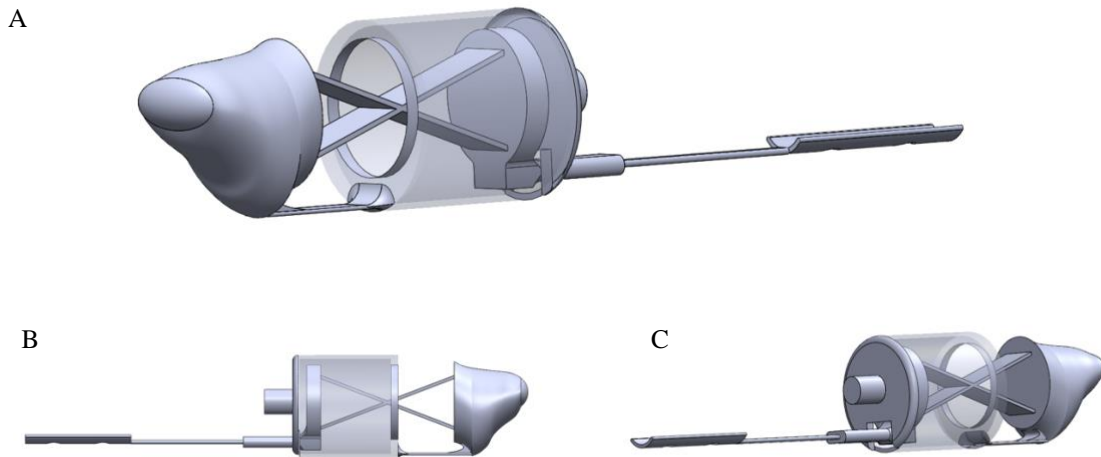


Figure 7: Compliant Thumb Design with cruciform for IP joint. A: Front view B: Side profile. C: Back view. The length of the whole implant is 70.5mm. The length from the proximal phalanx to thumb tip is 32.5mm. The diameter of the implant is 14.56mm diameter. The cruciform is 5mm wide, 20.34mm in length, and 0.4mm thick. The flat compliant below the cruciform is 5mm wide, 20.34mm in length, and 0.4mm thick. The flat compliant rotating parallel to the MCP is 16mm length, 1mm wide, and 0.3mm thick.

The benefit of a cruciform design is that it is easier to manufacture and has a fixed center of rotation, allowing a more feasible design for a surrounding shield. However, when deformed, stress concentration occurs at the center of cruciform, where the x crosses, limiting the range of motion.

In comparison to the cruciform, the cross-pivot design is more challenging to manufacture. Additionally, the blades would require shorter widths (2.75mm), which can cause torsion when

load is applied. However, cross-pivot designs have a larger ROM since there are no stress concentrations in the center of the blades.

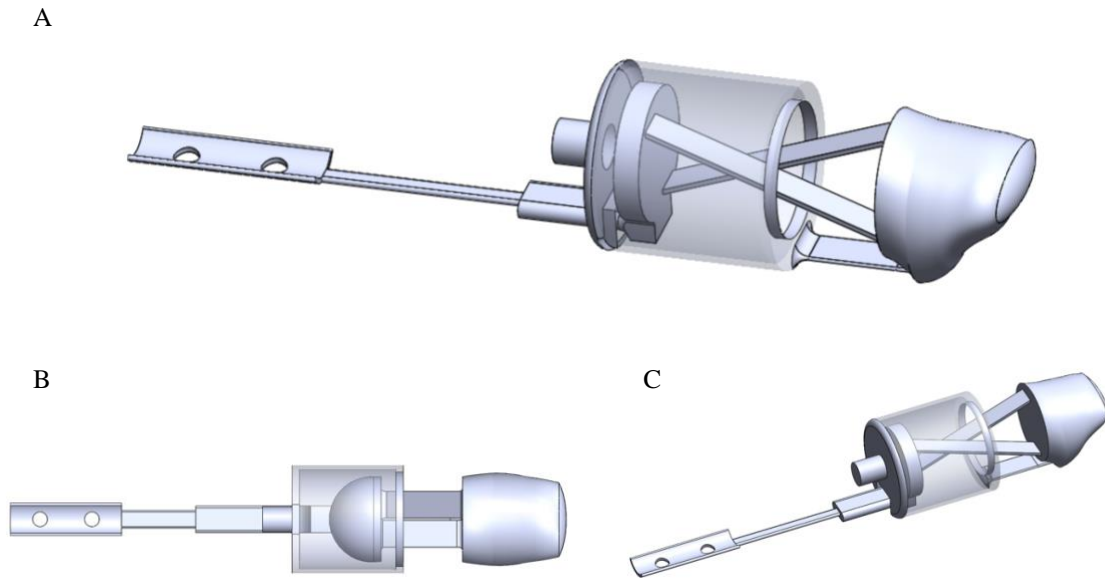


Figure 8: Cross-pivot thumb design. A: Front view B: Top profile. C: Back view

Materials were selected based on these mechanical properties as well as biocompatibility. Titanium (Ti) and Polyethylene (PE) are common implant materials used for medical and/or dental implants, including artificial joints and bone fixators. The benefit of Ti is that it is highly corrosion resistant and has high biocompatibility. Titanium also allows for osseointegration with the bone (Van Noort 1987). Commercially pure Ti (Ti CP) and extra low interstitial Ti-6AL-4V are two common Ti-based implant biomaterials that are classified as biologically inert. Ti CP, Ti6Al4V, High density polyethylene (HDPE), low density polyethylene (LDPE), and ultra-high molecular weight polyethylene (UHMW), were analyzed for range of motion in Abaqus FEA.

As mentioned in the hinge thumb designs, a coverage of the IP joint can be designed to shield the mechanism from the skin flap as shown in Figure 9.



Figure 9: Coverage design of cruciform IP joint.

2.4 Abaqus FEA Simulation Results

Abaqus finite element analysis (FEA) was used for various width thickness in the cruciform to determine the range of motion when unloaded. Forces that are applied to produce bending motion range between 0.3N to 1N. For cruciform design, Ti and UHMW both exceeded their yield stresses before reaching 40° ROM. Low density polyethylene (LDPE) and High-density polyethylene (HDPE) were both simulated and ROM was analyzed for varying cruciform thicknesses.

For LDPE, a yield strength of 16.27 MPa and Young's modulus of 172 MPa was used (Matweb 2018). For HDPE, a yield strength of 43 MPa and Young's modulus of 560 MPa was used (MatWeb LLC 2014). A Poisson ratio of 0.46 was used for both LDPE and HDPE (PolymerDatabase 2007). The implant fixation and loading points are shown in Figure 10.

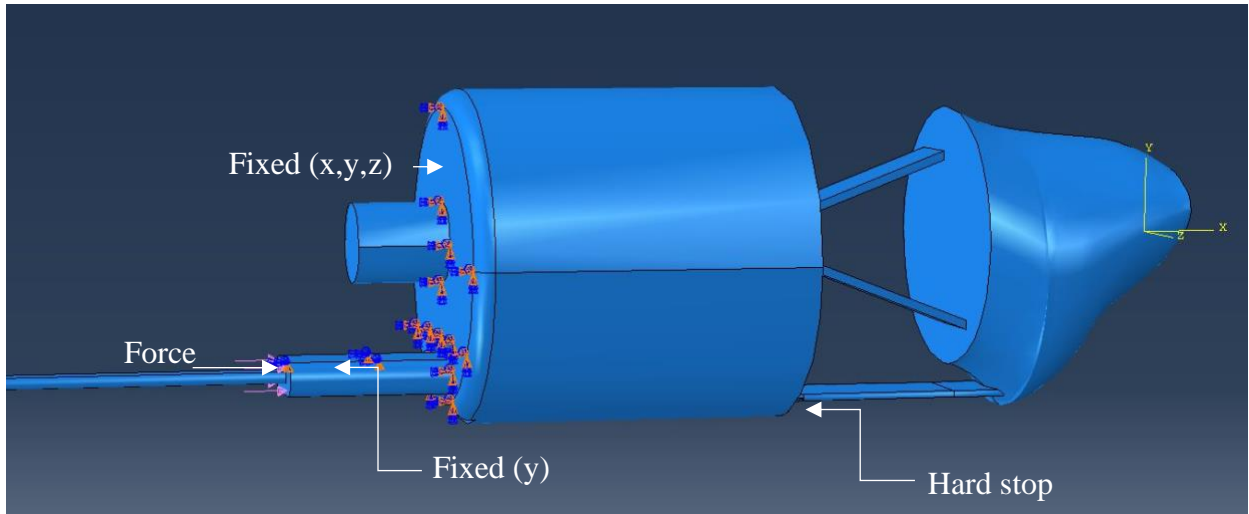


Figure 10: Boundary conditions and load for Abaqus simulations

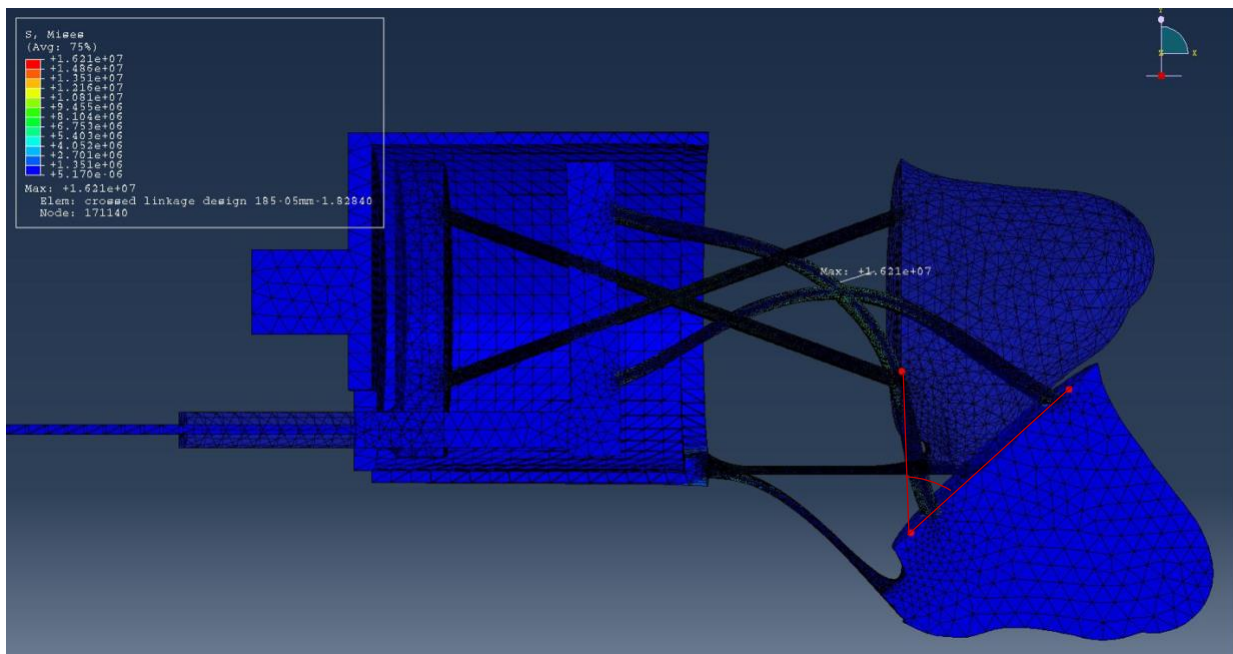


Figure 11: Before and after deformation of flexure. Implant design with 0.5mm cruciform thickness and 0.3mm bottom flat flexure thickness with LDPE. At yield stress, range of motion is 50°. The red dots and line indicate the angle that was measured for range of motion.

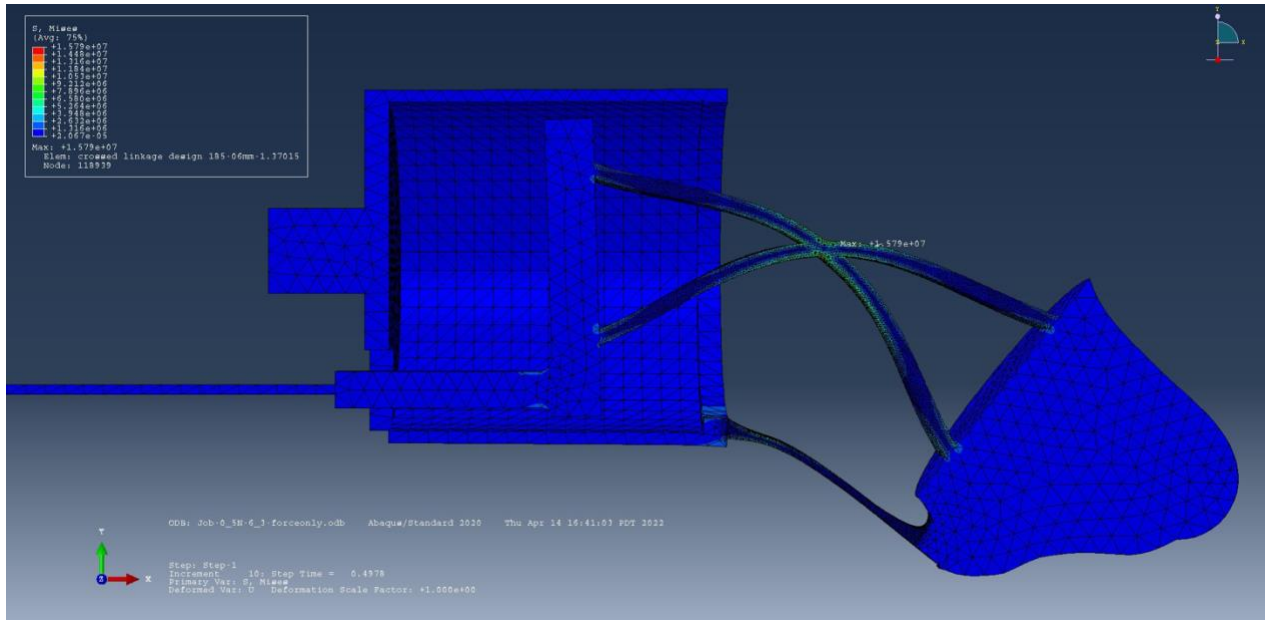


Figure 12: Implant design with 0.6mm cruciform thickness and 0.3mm bottom flat flexure with LDPE. At yield stress, range of motion is 40°.

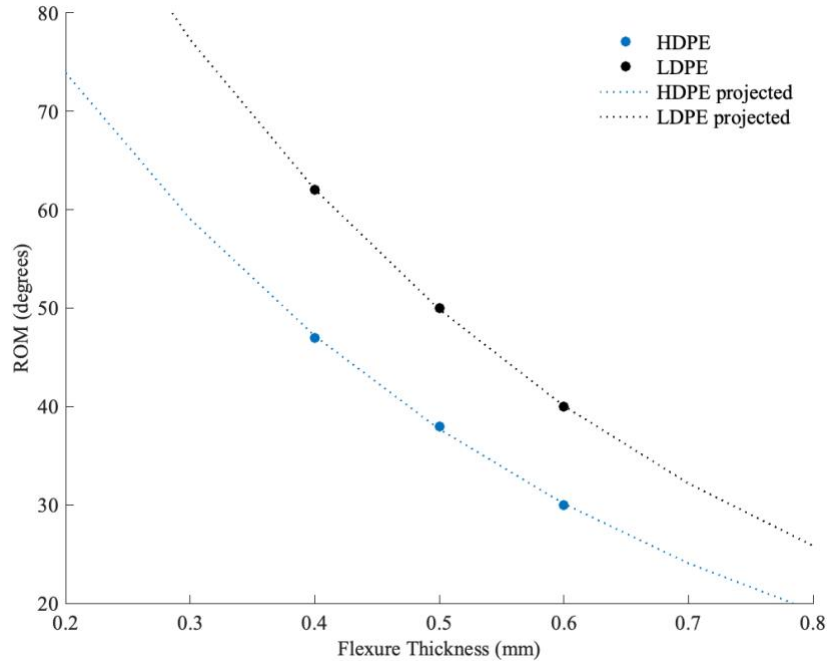


Figure 13: ROM at Yield Stress for LDPE and HDPE of 0.4, 0.5, and 0.6mm cruciform thicknesses.

As mentioned in the compliant mechanism thumb design section, a targeted ROM of around 40° is reasonable to achieve opposition grasp (Li and Tang 2007). For LDPE, any thicknesses below 0.6mm achieved this ROM as shown in the graph above. For HDPE, only thicknesses below 0.4mm achieved the desired ROM.

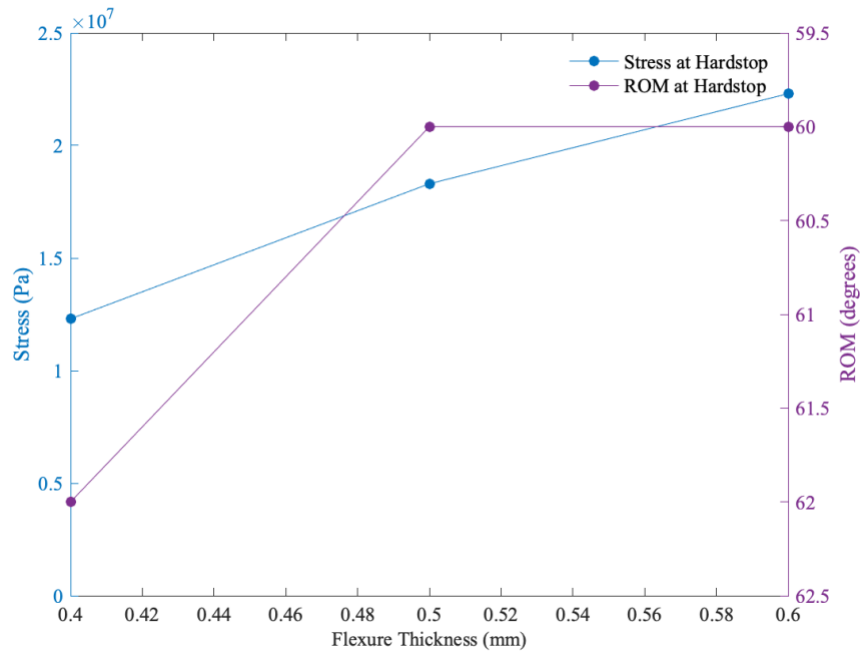


Figure 14: Stress and ROM at hard stop of 0.4, 0.5, and 0.6mm cruciform thicknesses.

Cruciform width of 0.4 to 0.5mm resulted in decreasing ROM as thickness increased, but limited changes in ROM was observed from 0.5mm to 0.6mm. On the other hand, stress increased linearly as thickness increased.

FEA on the cross-pivot design was also analyzed for thickness of 0.4mm. The thickness of the flat flexure below the IP flexure was increased to 0.6mm due to simulation failures for anything lower than 0.6mm. The ROM achieved at the hard stop was 70° and the stress was at 8.48 MPa for LDPE (Figure 15).

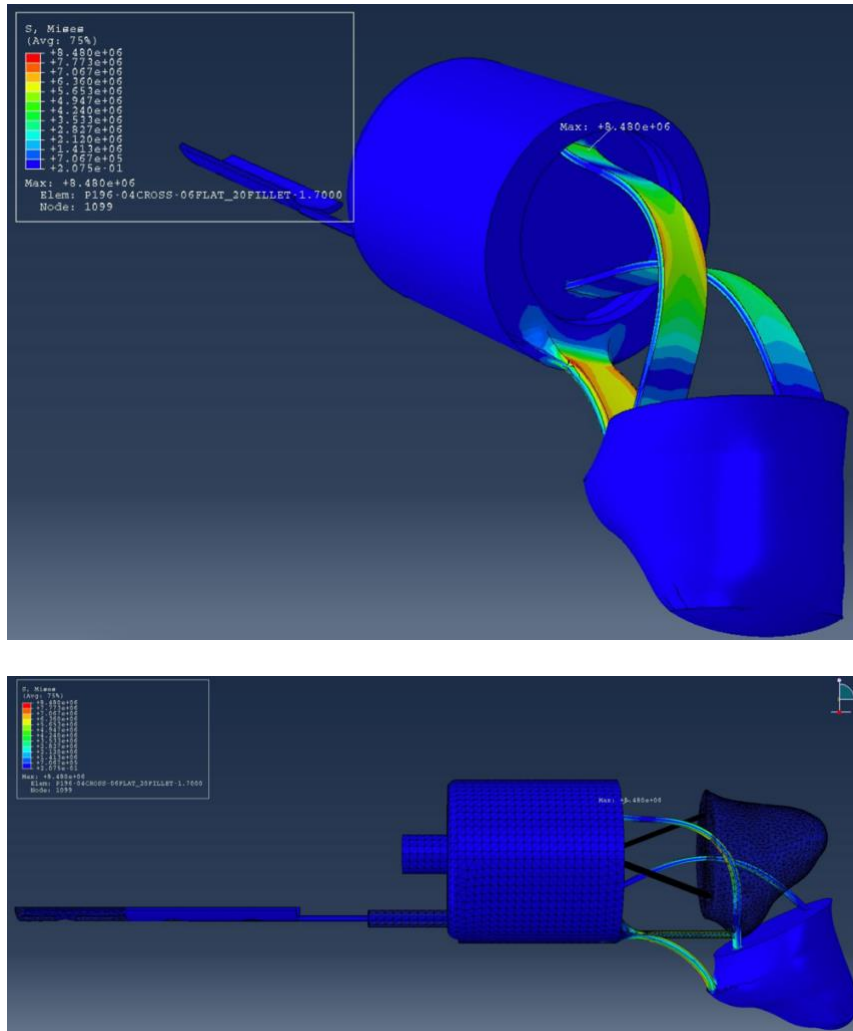


Figure 15: FEA results of cross pivot design. Max stress: 8.48 MPa.

There was no load placed on the thumb tip in the simulations analyzed for ROM data. It must be noted that under significant load conditions, buckling of the blades could occur. An inverted compliant design, where the load causes tension instead of compression would ease this issue. Inverting the blades would increase complexity in the design, material, size, and manufacturing. Under our current design constraints, this is quite challenging to incorporate, but the idea will be further explored in future works.

Loaded results were analyzed for the cross-pivot design since the stress at the flexures were a lot lower than that of the cruciform design. In the image shown below, a 0.1N load at the thumb tip and 0.3N force at the MCP flexure was applied to initiate the linkage mechanism.

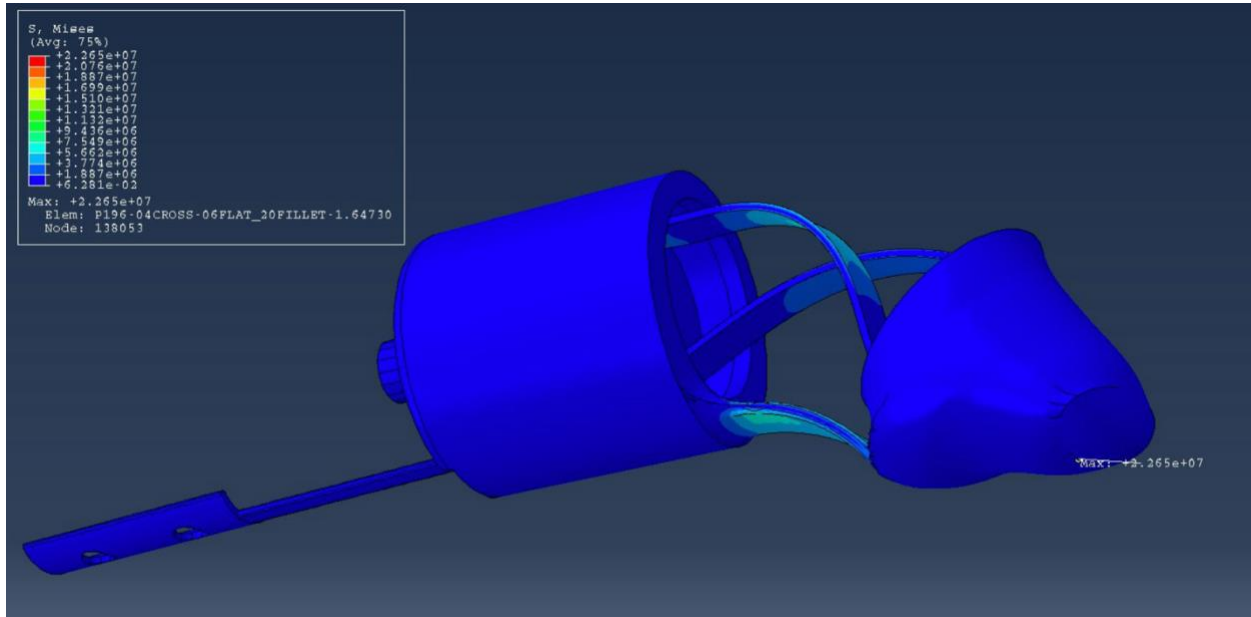


Figure 16: Loaded results of cross pivot design.

Under these low loading conditions, buckling and the stress in the flexure remained low. The stress was mostly concentrated in the thumb tip which can be made of Ti to sustain more stress. Although compliant mechanisms decrease wear of material, the articulating hinge design would allow for higher loads.

2.5 Implant in Cadaver

To test the implant motion in a human hand, a cadaver hand was dissected and the prosthetic hinge thumb design was implanted into the human hand. The tendons, nerves, and muscles were identified before amputating the thumb at the proximal phalanx (Figure 17).

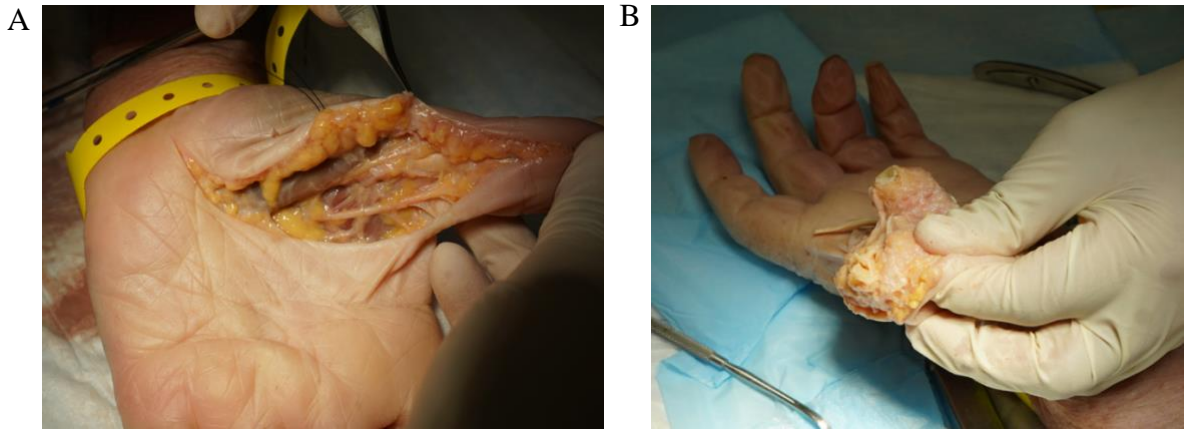


Figure 17: A: Flexor pollicis brevis muscle, A1 pulley tendon, palmar digital nerves. B: Amputated proximal phalanx.

The hinge thumb prototype was 3D printed and the hinges were assembled using wires. The implant was fixated using bone cement into the medullary canal of the proximal phalanx and screwed into the volar side of the metacarpal bone (Figure 18).

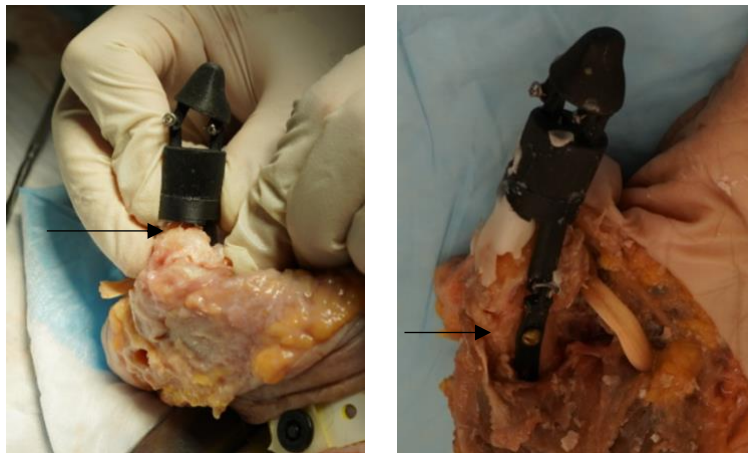


Figure 18: Arrows showing implant fixation and insertion points.



Figure 19: Opposition motion of the implant, right image shows implant under the skin.



Figure 20: Thumb in extension, right image shows extension of implant under the skin.



Figure 21: Thumb in flexion, right image shows flexion of implant under the skin.

This dissection successfully showed restoration of opposition motion, extension, and flexion through the thumb implant design in the human hand (Figure 19, Figure 20, Figure 21).

2.6 Conclusion

In summary, this chapter describes an implantable prosthetic thumb design that integrates with the bone and restores joint motion. The range of motion of the hinge design is 60°, which is more than sufficient for opposition grasp. A surgical method is also described to surround the prosthetic thumb with sensate skin. This method restores natural sensation in amputated regions, which is a dramatic unmet need in current prosthetic devices.

This solution has the potential to extend to partial hand amputations and even full hand amputations. This can revolutionize the standard of care for people with hand amputations because it provides a solution to replace functional components associated with the natural hand anatomy and physiology. Presently, there is not a single finger prosthetic device that provides solutions in all of the following areas: direct integration of the prosthesis with the human body, cosmesis, function, sensation, and stability. This solution would create an illusion of a complete natural limb replacement.

Chapter 3: Rat Model

3.1 Introduction

As a first step in confirming the feasibility of our human model, it is necessary to validate our surgical solution and test the viability of this device with living skin. One of the key factors that might limit our solution to rebuilding the amputated finger with a skin covered prosthetic device is the reaction of the skin to the non-biological material of the prosthesis. As such, we want to study how the implant motion and material, as well as surgical techniques, would allow the skin to remain healthy over time.

We have designed a surgical approach for this study that does not require amputation of rat limbs. Instead, we will move skin from one portion of the body to another part of the body and use it to cover a piece of synthetic material that has similar properties to our proposed prosthetic finger. To do so, we must first design a rat model that represents the human model. In the human model, as described in Chapter 2, a rotation flap, with the blood vessel still intact, is rotated onto the recipient site and ‘tubularized’ around the implant. In this chapter, we will validate a rat model involving the rotation and ‘tubularization’ of a flap.

The IACUC protocol, ARC-2021-059, was approved by the Division of Laboratory Animal Medicine (DLAM) at the University of California, Los Angeles (UCLA). The rat model was designed in collaboration with Dr. Kodi Azari and Dr. Lauren Wessel with the help of surgical residences Dr. Nirbhay Jain and Dr. Meaghan Barr. The primary surgeons for the rat surgeries were Dr. Kodi Azari and Dr. Lauren Wessel.

3.2 Specific Aims

Our goal in this study is to create a rat model that would allow transposition of skin from one part of the rat body for use in covering an implanted prosthesis. This rat study will allow us to determine how to best design this new surgical methodology while leveraging existing techniques in reconstructing a skin envelope that will support years of implantation without wearing through the skin or becoming infected.

The results of this rat model will be used in future studies to determine if the prosthesis will cause extrusion in prelaminated skin and if coating or muscle wrapping of the prosthesis is needed.

Our aims for the rotation flap model are as follow:

1. Flap is large enough to cover the implant but small enough to prevent necrosis.
2. Flap is 'tubularized' to imitate the human flap surrounding thumb.
3. Flap has sufficient motion caused by the rat's daily movements to allow for motion of implant under the skin.

3.3 The Epigastric Flap

The epigastric fasciocutaneous flap is most widely used for teaching purposes due to constant and sizeable vascular anatomy, redundancy of skin, and ease of dissection. The epigastric flap is supplied by the superficial epigastric artery (0.3-0.5mm) and vein (0.6-0.8mm), which originate from the femoral artery and vein (Casal et al. 2017), located in the region of the ventrolateral abdominal wall. The length and width of the flap can be up to 5cm and 3cm, respectively. (Casal et al. 2017)(Karacalar et al. 2000)

The superficial epigastric artery divides into a lateral and medial branch before dividing into capillary networks that supply most of the epigastric region (Casal et al. 2017). The epigastric nerve runs along the epigastric vessels in a tightly bound neurovascular bundle (Kostakoğlu et al. 1994).

Some applications of this flap include transfer of the fasciocutaneous epigastric free flap to the neck of a rat (Casal et al. 2017), sensory recovery of the epigastric flap after nerve injury (Tomita et al. 2020), and the comparison of neurovascular changes in innervated and denervated skin grafts (Kostakoğlu et al. 1994). In our experiment, the epigastric flap is going to be used as a rotation flap.

3.4 Materials and Methods

3.4.1 Flap Elevation and Rotation Surgery

The surgical procedures were designed and tested on four rat cadavers prior to starting live rat procedures. Male Lewis Rats weighing around 300g to 480g were used. Meloxicam and Gabapentin were administered to the rats one day before the operation. At least one hour prior to the procedure the rats were administered 72 hours sustained release of Buprenorphine, regular Buprenorphine, Meloxicam, Gabapentin, and Lactated Ringer's Solution (LRS). Rats were first anesthetized using long-duration Isoflurane. During anesthesia, a standard heating pad was used to provide heat to the rats.

The location of the epigastric vessel was found by feeling the pulse of the vessel through the skin. Flap geometry was then drawn with a sterile pen. Incisions were made in the distal epigastric regions in the shape of a 'tennis racket' (close to the groin and hind leg, approximately a 4cm x 3cm skin flap). The 'racket handle' was centered along the epigastric vessel.

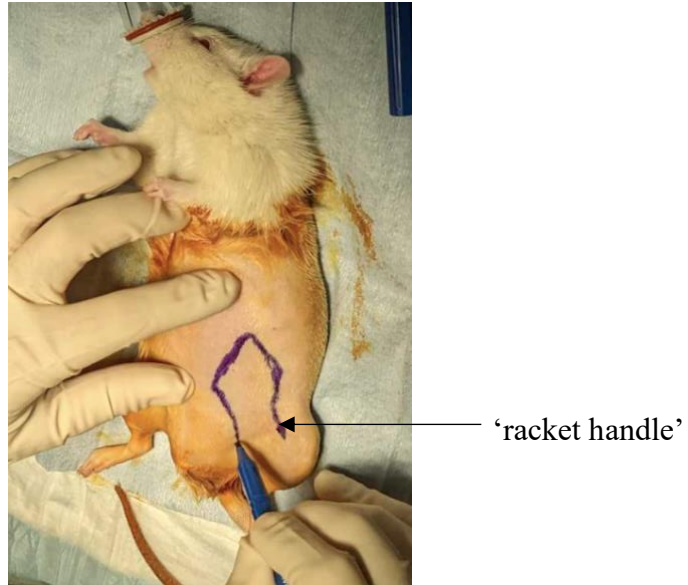


Figure 22: 'Tennis racket' shape flap drawn in the epigastric region.

Incisions started on the medial side of the 'tennis racket' where the flap was elevated and separated from the underlying fascia. Incisions were then made on the lateral side of the 'tennis racket' and the whole flap was elevated with the distal end of the 'racket handle' still intact. The epigastric vessel was not clipped. Bupivacaine was splashed onto the elevated flap and donor site.

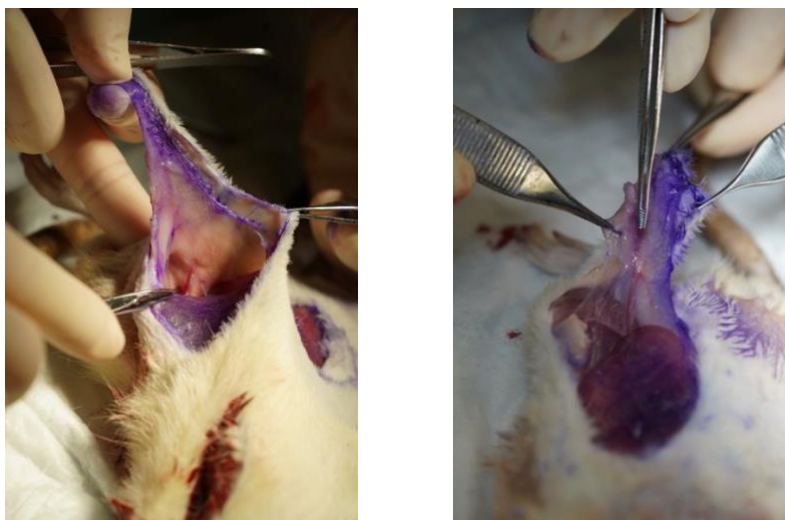


Figure 23: Images of epigastric vessel from dissection of rat cadavers

4-0 Resorbable poliglecaprone sutures were used with suture patterns that don't exteriorize the suture material to prevent the rats from chewing off the sutures. After the flap was elevated off the epigastric region, the donor site incision was closed. For the elevation flap control rats, after the flap was isolated from the fascia, it was placed back to its original site and the incision was closed. For the rotation flap control group, the flap was 'tubularized' (folded and sutured in a side-to-side fashion starting with the distal end). For the experimental group, the 'tubularized' flap was rotated around 50° to 80° on to the lateral side of the abdominal region. An incision was made where the distal end of the 'tubularized' flap was tacked onto the skin. The 'tubularized' flap was then sutured epidermis-to-epidermis at the recipient site.

Post-operation medications included Meloxicam, Gabapentin, Enrofloxacin, and 72-hour sustained release Buprenorphine. Vetericyn spray and DietGel were also given to the rats.

3.4.2 Flap Motion Analysis

To determine if this rat model will accurately represent how the skin reacts to the motion of implant under the skin, three points on the flap were tracked using tracker software from Physlets. After the rat was euthanized, three points were drawn on the 'tubularized' flap on its most distal, proximal, and center region as shown in the image below.

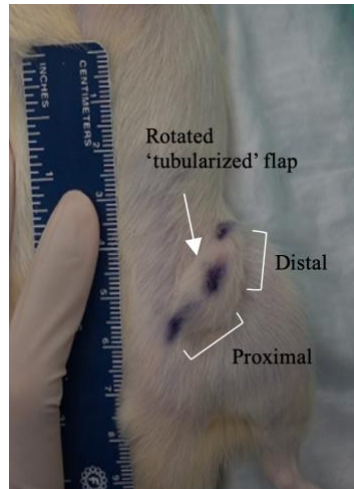


Figure 24: Bottom, center, and top points tracked on the rotated flap.









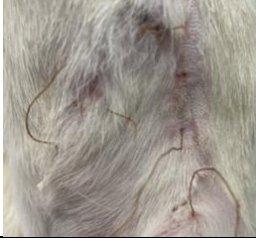

The hind leg was rotated and stretched for four cycles while the three points were tracked in 2D space. The distances between the bottom and center point (proximal strain) and between the center and top point (distal strain) were computed. Strain was found by normalizing the distances with the distance at time 0.

3.5 Results and Discussion

3.5.1 Flap Elevation and Rotation Surgery

In the flap elevation control group, two rats underwent flap elevation surgery, where the flap was elevated and placed back to the original spot. For rat #2, 3M Vetbond Tissue Adhesive was used on the incision sites. No necrosis was found on both rat flaps. As displayed in Table 2, the incision site for rat #1 was a slightly larger and proximal, whereas the incision site for rat #2 was more distal. The results from these two rats show that the flap region is viable and the epigastric vessel provides sufficient vascularization to the flap region.

Table 2: Images of control group 1 rats with flap elevation, from Day 1 to Day 10+ post-op.



	Rat #1	Rat #2
Surgery Day		
Day 1 post-op		
Day 3 post-op		
Day 6 post-op		
Day 10+ post-op		







In the second group of rats, six rats subsequently underwent flap elevation, rotation and ‘tubularization’ procedures. Rat #3 was euthanized the day after surgery because of significant bleeding through the incision sites as shown in Table 3. A necropsy was performed post-euthanization and it was found that the sutures were still intact, indicating that the bleeding

could have originated from one of the vessels in the epigastric flap that were clipped during surgery. However, no hematoma was found. Cautery pens were used for the subsequent surgeries and no significant bleeding was found in the following rats. The first rotation flap model (rat #3) had a large rotation angle (~130°) which could have caused the vessel to retract due to the additional movement of the hind leg. To remain conservative, a new flap rotation model (2) was designed for the subsequent rats (#4,5).

The new flap model (2) had a rotation angle of around 80°, where the ‘tubularized’ flap was rotated and tacked onto the posterior of the hip bone. This would not allow for an articulating implant design, so the design was changed to two separate parts that moved forwards and backwards from each other as the hind leg stretched and retracted. To reduce the chances of the rat chewing the tacking site sutures, an incision was made on the posterior of the hip bone so the flap can be sutured epidermis-to-epidermis to allow for skin growth from the flap to the tacking site. No bleeding was found in rat #4 post-op. However, the rat did chew on the sutures causing dehiscing of the flap as shown in the post-ethanization image below. Since the flap was opened and vulnerable for infection, the rat was euthanized.



Table 3: Images of rotation flap model 1 vs. rotation flap model 2











	Rat #3	Rat #4
Surgery Day		





Surgery Day		
Post-euthanization		
Necropsy		

To prevent the rat from chewing on the sutures, subcuticular suture patterns were used in the subsequent rats.

Table 4: Images of rotation model 2 vs. rotation model 3.

	Rat #5	Rat #6
Surgery Day		

Day 1 post-op		
Day 2 post-op		
Day 4 post-op		
Day 5 post-op		
Day 6+ post-op	 <p data-bbox="737 1661 885 1701">(Necropsy)</p>	 <p data-bbox="1032 1661 1239 1701">(Day 9 post-op)</p>

Day 6+ post-op	 <p data-bbox="737 520 885 554">(Necropsy)</p>	 <p data-bbox="1024 520 1247 554">(Day 13 post-op)</p>
Day 6+ post-op	 <p data-bbox="737 882 885 915">(Necropsy)</p>	 <p data-bbox="1024 882 1247 915">(Day 18 post-op)</p>






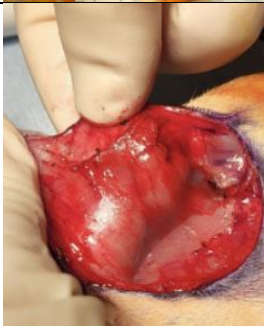
No dehiscing of the flaps occurred after subcuticular patterns were used. Discoloring of the flap was observed first day post-op and necrosis was observed on the distal end of Rat #5 starting day two post-op. A necropsy was performed and necrosis was found in the peripheral region of the flaps as shown in the images in table above. There are several hypotheses for why necrosis occurred in this rat. Firstly, the epigastric vessel of this rat was observed to be less robust than the previous rats on the day of surgery. Rotation and torsion of the vessel could have also caused kinking of the vessel. It is unlikely that the flap length was too long because necrosis was not observed for flap elevation control rats.











Rotation and torsion of the vessel were most likely the reasons for necrosis. As a result, rotation model 3 was designed to have a smaller rotation angle, of around 50°, without any torsion of vessel. A smaller rotation angle is intended to decrease the piston motion of the flap when the prosthesis will be implanted. However, movement in the flap was still observed when the rat stood on its hind leg to eat/ drink water (food and water is placed on the top of the cage).









Incisions sites of the rats were fully healed by day 18 post-op and no necrosis was observed in the flap.

To confirm the viability of this model, two additional rats underwent the same rotation flap surgery.

Table 5: Images of Rotation model 3.

	Rat #7	Rat #8
Flap Location (Surgery Day)		
Flap Size (Surgery Day)		
Epigastric Vessel (Surgery Day)		

<p>Extension (Surgery Day)</p>		
<p>Flexion (Surgery Day)</p>		
<p>Day 1 post-op</p>		
<p>Day 2 post-op</p>		
<p>Day 4 post-op</p>		

Day 5 post-op		
Day 7 post-op		
Day 13 post-op		
Day 18 post-op		

On surgery day, rat #8 was observed to have more fat tissue, so the epigastric vessel was harder to identify as shown in the image in the table above. Mild discoloring of the flap occurred on day two post-op. The rat started chewing on the flap day six to seven post-op. Treatment was given to the rat and the flap successfully healed without necrosis.

3.5.2 Flap Motion Analysis

For the rat model to be a proper representation of the human model, there must be sufficient motion in the flap to allow the implant to piston. The following graphs show the strain between 3 points on the flap.

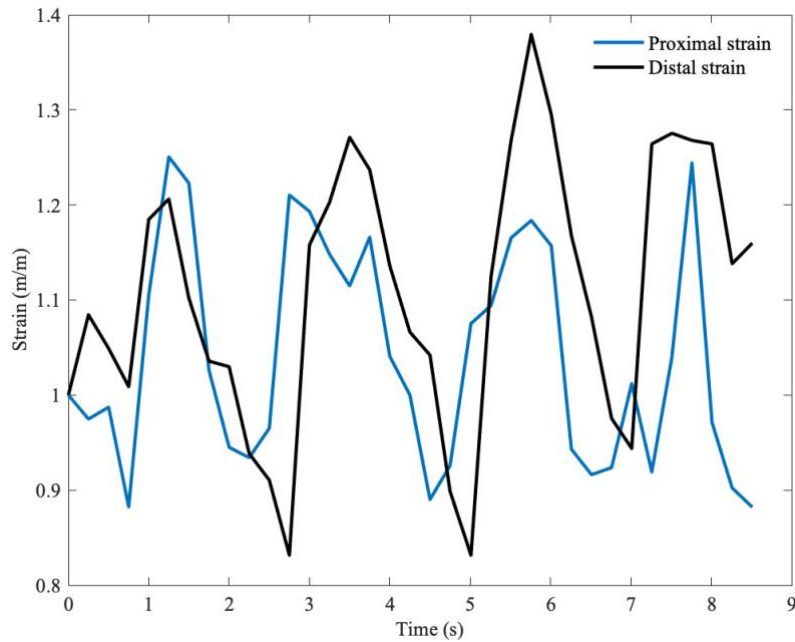


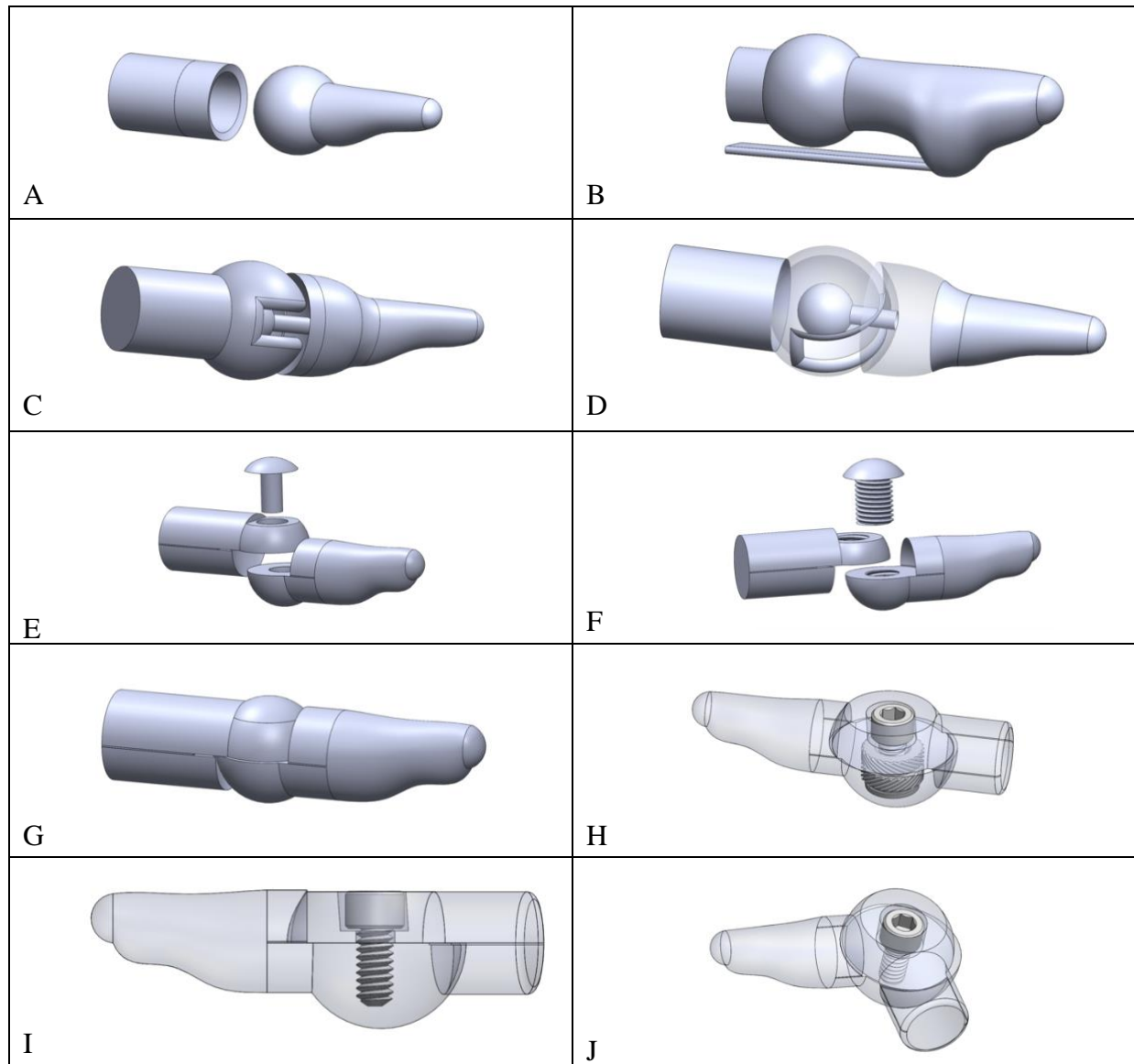
Figure 25: Changes of flap strain as hind leg rotates and stretches over 4 cycles. Blue line shows the strain between bottom and center points (proximal strain). Black line shows the strain between center and top points (distal strain).

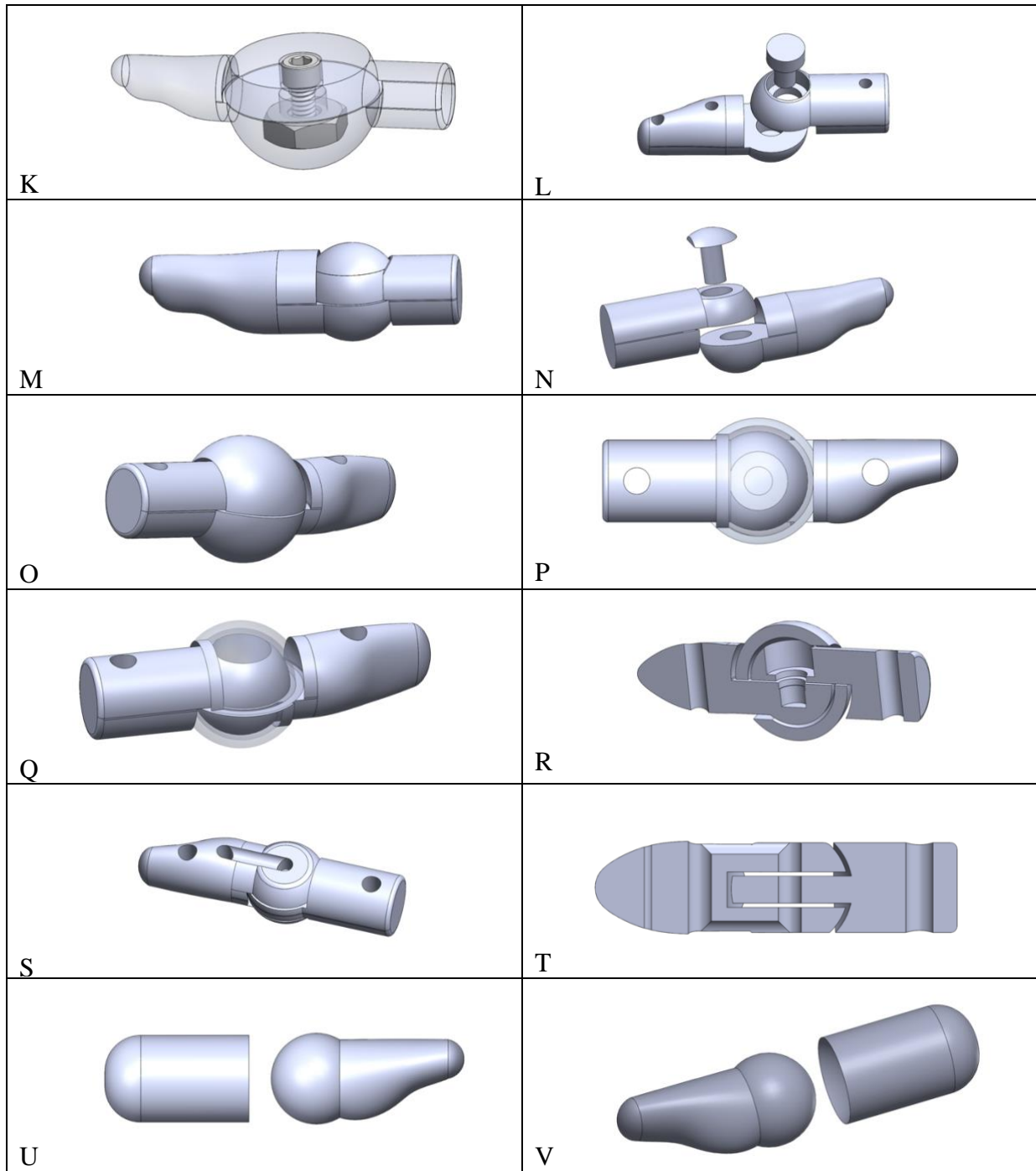
The graph shows a max strain of 1.38 and minimum of 0.83. These are conservative measurements of how much the flap will move in a live rat as this data is obtained solely through motion of hind leg. When the rat is active there should be flexion, extension, and rotation of the abdominal region, which would provide even more motion in the flap region.

3.6 Rat Implant Design

The goal of the rat prosthesis design is to implant a foreign material with similar shape of the human prosthesis. The implant should produce some motion underneath the skin to test for extrusion of the skin and fibrous ingrowth of the implant. The implants were modelled using Solidworks 3D CAD software.

Table 6: Design iterations of rat implant.





The largest constraint of the rat implant design is the size of the implant. As the size of the implant increases, a larger flap is required, increasing the chance of necrosis. The final implant size is around 4.88mm in diameter and 17.2mm in length. Images A to T are designed for rat rotation model 1 as described above.

Initial designs of the rat implant include 2 parts that were articulating against one another (Table 6). Compliant mechanisms were not used in the rat implants. Due to the limited space, manufacturing a flexure with that size and proper mechanical properties would be very challenging. Several design prototypes were 3D printed using a Markforged MarkTwo 3D printer and the Onyx™ material. Several types of connection of the articulating surfaces were prototyped. As shown in Table 6, this includes: a ball joint (C,D), pin and medical grade glue (cyanoacrylate glue) (E,L,N), screw (F,I,J), screw and threaded insert (H), screw and bolt (K), and wire (T). Ideally the implant joint would not be porous whereas the rest of the implant should be porous to increase fibrous ingrowth. A shield is designed around the joint and can be made from a non-porous material (O,P,Q) and glued onto the implant using medical cyanoacrylate glue.

Due to the limitations of rat flap size, manufacturing capabilities, and changes in rotation model, the implant design was simplified to 2 parts that can piston against each other. The final design of the implant is shown in images U and V (Table 6). To minimize extrusion of the implant, a high porosity material was chosen to allow for tissue ingrowth and stabilization of the implant. Implants were manufactured with porous high-density polyethylene (HDPE) (Anatomics StarPore®) as shown in Figure 26 and implanted into two rats as show in Figure 27.

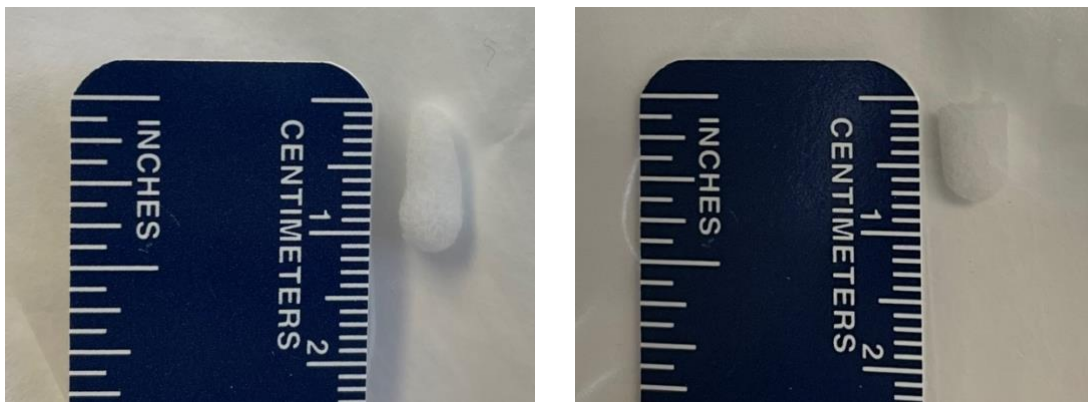


Figure 26: Implants part 1 and 2 manufactured by Anatomics Starpore material (porous HDPE).

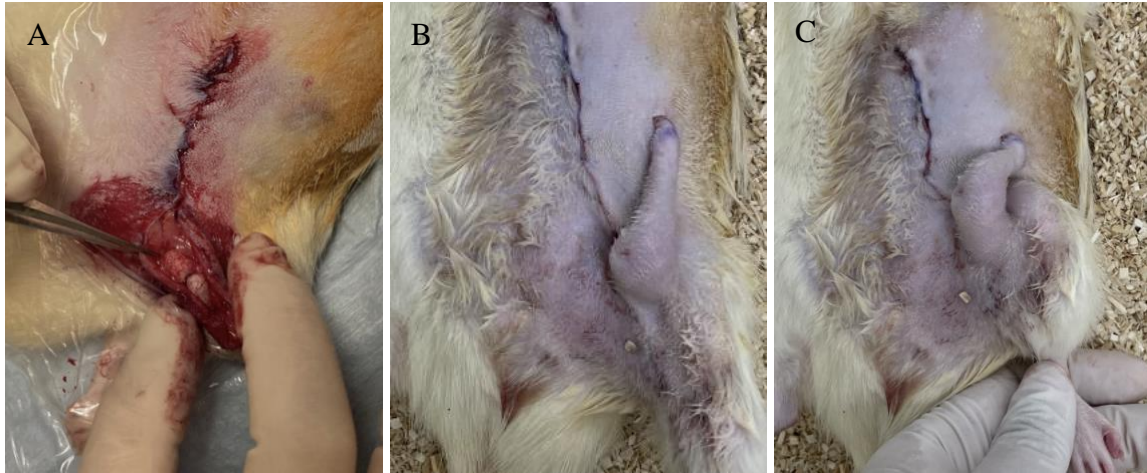


Figure 27: A: Implants inserted in the ‘tubularized’ rotated flap. B: Closed ‘tubularized’ flap with implant when hind leg is extended. C: Closed ‘tubularized’ flap with implant when hind leg is flexed.

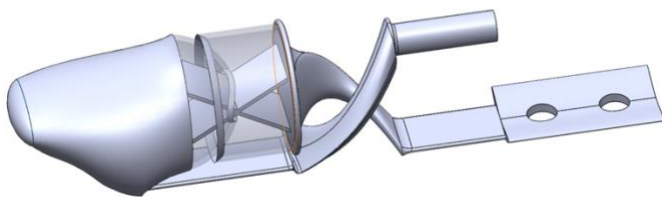
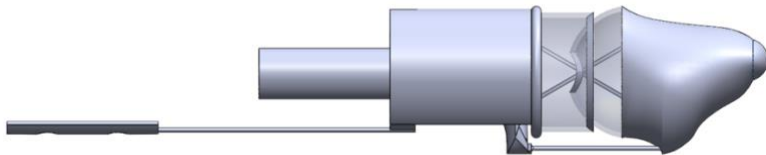
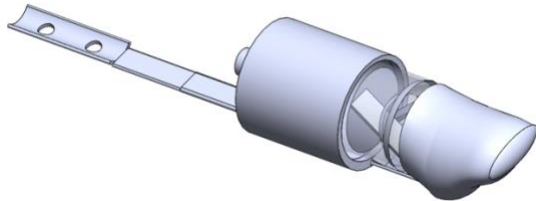
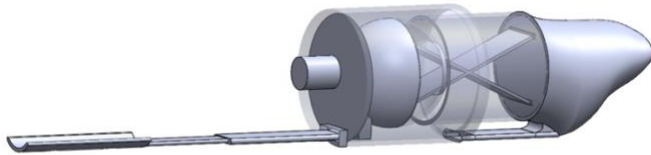
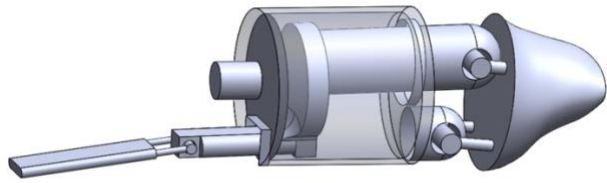
3.7 Conclusion

The findings in this study provide a viable rat rotation model for a ‘tubularized’ flap with sufficient motion for prosthesis implantation. Two rats successfully underwent flap elevation surgery, and three rats successfully underwent flap rotation (model 3) surgery. No necrosis was found in all 5 rats.

Future studies would include analysis of prelaminated prosthesis and how it affects tissue ingrowth and extrusion. An experimental group of rats that undergo implant prelamination procedure prior to rotation of flap will be compared with negative control group with implant directly inserted in ‘tubularized’ rotation flap. Reinnervation of the rotated flap will also be tested to verify restoration of sensation in the rotated flap. The results of this study would determine if prelamination can decrease incidence of extrusion and increase fibrous ingrowth.

Appendices

Previous thumb designs:



Bibliography

- Babaei, Alireza, Mohammad Reza Safarinejad, Elham Iran-Pour, and Farhat Farrokhi. 2010. "Evaluation of the Most Accepted Techniques." 7(2): 8.
- Bajaj, Ajay et al. 2021. "Soft Hand Exoskeleton for Adaptive Grasping Using a Compact Differential Mechanism." *Lecture Notes in Mechanical Engineering*: 733–46.
- Branemark, Per Ingvar. 1983. "Osseointegration and Its Experimental Background." *The Journal of Prosthetic Dentistry* 50(3): 399–410.
- Brånemark, Rickard, P. I. Brånemark, Björn Rydevik, and Robert R. Myers. 2001. "Osseointegration in Skeletal Reconstruction and Rehabilitation: A Review." *Journal of Rehabilitation Research and Development* 38(2): 175–81.
- Brenner, Michael J. et al. 2006. "Repair of Motor Nerve Gaps with Sensory Nerve Inhibits Regeneration in Rats." *Laryngoscope* 116(9): 1685–92.
- Brown, Paul W. 1982. "Less than Ten—Surgeons with Amputated Fingers." *Journal of Hand Surgery* 7(1): 31–37. [http://dx.doi.org/10.1016/S0363-5023\(82\)80010-5](http://dx.doi.org/10.1016/S0363-5023(82)80010-5).
- Capek, Karel D., Byron D. Hughes, and Glenn D. Warden. 2018. "Functional Sequelae and Disability Assessment." *Total Burn Care: Fifth Edition*: 673-678.e1.
- Casal, D et al. 2017. "A Model of Free Tissue Transfer: The Rat Epigastric Free Flap." *J. Vis. Exp* (119): 55281. www.jove.com/url=https://www.jove.com/video/55281 (May 17, 2021).
- Chiang, Yuan Cheng. 2006. "Combined Tissue Expansion and Prelamination of Forearm Flap in Major Ear Reconstruction." *Plastic and Reconstructive Surgery* 117(4): 1292–95.
- Crainiceanu, Zorin et al. 2016. "Innovative Method of Titanium Plate Use for Morphological and Functional Human Face Reconstruction." *Materiale Plastice* 53(3): 518–21.
- Dijkstra, Jeroen R., Marcel F. Meek, Peter H. Robinson, and Albert Gramsbergen. 2000.

- “Methods to Evaluate Functional Nerve Recovery in Adult Rats: Walking Track Analysis, Video Analysis and the Withdrawal Reflex.” *Journal of Neuroscience Methods* 96(2): 89–96.
- Doctor, Azmat M., Jimmy Mathew, Sunderraj Ellur, and Anusham A. Ananthram. 2010. “Three-Flap Cover for Total Hand Degloving.” *Journal of Plastic, Reconstructive and Aesthetic Surgery* 63(4): e402–5. <http://dx.doi.org/10.1016/j.bjps.2009.10.007>.
- Fermi, Matteo et al. 2021. “Prelaminated Flaps in Head and Neck Cancer Reconstructive Surgery: A Systematic Review.” *Microsurgery* 41(6): 584. [/pmc/articles/PMC8518088/](https://pubmed.ncbi.nlm.nih.gov/34818088/) (March 26, 2022).
- “Hand Anatomy | HealthEngine Blog.” 2008. <https://healthengine.com.au/info/hand#Cc> (February 15, 2021).
- Herndon, D. N. et al. 1989. “A Comparison of Conservative versus Early Excision. Therapies in Severely Burned Patients.” *Annals of Surgery* 209(5): 547–53. <https://pubmed.ncbi.nlm.nih.gov/2650643/> (February 27, 2021).
- Imbinto, I. et al. 2018. “The S-Finger: A Synergetic Externally Powered Digit with Tactile Sensing and Feedback.” *IEEE Transactions on Neural Systems and Rehabilitation Engineering* 26(6): 1264–71.
- Imbinto, Ilario et al. 2016. “Treatment of the Partial Hand Amputation: An Engineering Perspective.” *IEEE Reviews in Biomedical Engineering* 9: 32–48.
- Inbal, Rivka et al. 1987. “Collateral Sprouting in Skin and Sensory Recovery after Nerve Injury in Man.” 28: 141–54.
- Jan de Cubber, Zaventum. 2007. “Patent Application Publication (10) Pub . No .: US 2007 / 0213831 A1.” *Us 2007 / 0213831 a1* 1(60): 19–21.

- Karacalar, A., O. Idil, Z. Kahveci, and M. Özcan. 2000. "The Nervenous (or Adiponenvenous) Epigastric Flap in the Rat." *European Journal of Plastic Surgery* 23(5): 283–88. <https://link.springer.com/article/10.1007/s002380000133> (May 11, 2021).
- Kawashima, Takao et al. 1989. "Intraoral and Oropharyngeal Reconstruction Using a De-Epithelialized Forearm Flap." *Head & Neck* 11(4): 358–63. <http://doi.wiley.com/10.1002/hed.2880110413> (February 12, 2021).
- Kostakoğlu, N. et al. 1994. "Free Sensate Secondary Skin Flaps: An Experimental Study on Patterns of Reinnervation and Neovascularisation." *British Journal of Plastic Surgery* 47(1): 1–9.
- Kuiken, Todd A. et al. 2007. "Redirection of Cutaneous Sensation from the Hand to the Chest Skin of Human Amputees with Targeted Reinnervation." *Proceedings of the National Academy of Sciences of the United States of America* 104(50): 20061–66.
- Kunutsor, S. K., D. Gillatt, and A. W. Blom. 2018. "Systematic Review of the Safety and Efficacy of Osseointegration Prosthesis after Limb Amputation." *British Journal of Surgery* 105(13): 1731–41.
- Li, Zong Ming, and Jie Tang. 2007. "Coordination of Thumb Joints during Opposition." *Journal of Biomechanics* 40(3): 502–10.
- "Limb Loss Statistics." *Amputee Coalition*. <https://www.amputee-coalition.org/resources/limb-loss-statistics/#1> (March 1, 2021).
- Manktelow, Ralph T. 1986. "Toe to Thumb Transfer." *Microvascular Reconstruction*: 165–83. https://link.springer.com/chapter/10.1007/978-3-642-70329-4_25 (March 26, 2022).
- Manurangsee, P., C. Isariyawut, V. Chatuthong, and S. Mekraksawanit. 2000. "Osseointegrated Finger Prosthesis: An Alternative Method for Finger Reconstruction." *Journal of Hand*

Surgery 25(1): 86–92.

Matweb. 2018. “Overview of Materials for Low Density Polyethylene (LDPE).” *MatWeb database*: 27–28.

http://www.matweb.com/search/datasheet_print.aspx?matguid=b34a78d271064c4f85f28a9faf94045 (May 12, 2022).

MatWeb LLC. 2014. “Overview of Materials for High Density Polyethylene (HDPE), Extruded.” *MatWeb*: 0–3.

<http://www.matweb.com/search/datasheet.aspx?MatGUID=482765fad3b443169ec28fb6f9606660&ckck=1> (May 12, 2022).

Moran, Steven L., and Richard A. Berger. 2003. “Biomechanics and Hand Trauma: What You Need.” *Hand Clinics* 19(1): 17–31.

Van Noort, R. 1987. “Titanium: The Implant Material of Today.” *Journal of Materials Science* 1987 22:11 22(11): 3801–11. <https://link.springer.com/article/10.1007/BF01133326> (May 7, 2022).

Papadopoulos, Nikolaos A., Juergen Schaff, and Edgar Biemer. 2008. “The Use of Free Prelaminated and Sensate Osteofasciocutaneous Fibular Flap in Phalloplasty.” *Injury* 39(3 SUPPL.): 62–67.

Parrett, Brian M., and Julian J. Pribaz. 2010. “Prefabricated and Prelaminated Flaps.” In *Color Atlas of Burn Reconstructive Surgery*, Springer Berlin Heidelberg, 300–309.

https://link.springer.com/chapter/10.1007/978-3-642-05070-1_34 (February 10, 2021).

“Peripheral Neurological Recovery and Regeneration | PM&R KnowledgeNow.”

<https://now.aapmr.org/peripheral-neurological-recovery-and-regeneration/> (June 2, 2022).

Poeschl, P. W. et al. 2003. “The Radial Free Forearm Flap - Prelaminated versus Non-

- Prelaminated: A Comparison of Two Methods.” *International Journal of Oral and Maxillofacial Surgery* 32(2): 159–66.
- PolymerDatabase. 2007. “Poisson’s Ratio.” *Polymer* 56(1): 2007–2007.
[http://polymerdatabase.com/polymer physics/Poisson Table.html](http://polymerdatabase.com/polymer%20physics/Poisson%20Table.html) (May 12, 2022).
- Prabhu, Mahesh, Rajesh Powar, and Sanjitsingh R Sulhyan. 2013. “FDMA FLAP: A VERSATILE TECHNIQUE TO RECONSTRUCT THE THUMB.” *Int. J. Pharm. Med. & Bio. Sc.* www.ijpmbs.com (March 26, 2022).
- Pribaz, Julian J., Neil Fine, and Dennis P. Orgill. 1999. “Flap Prefabrication in the Head and Neck: A 10-Year Experience.” *Plastic and Reconstructive Surgery* 103(3): 808–20.
<https://pubmed.ncbi.nlm.nih.gov/10077069/> (February 10, 2021).
- Rajan, Bindu et al. 2003. “Epidermal Reinnervation after Intracutaneous Axotomy in Man.” *Journal of Comparative Neurology* 457(1): 24–36.
- Raspopovic, Stanisa et al. 2014. “Bioengineering: Restoring Natural Sensory Feedback in Real-Time Bidirectional Hand Prostheses.” *Science Translational Medicine* 6(222).
- “The Skin: Human Anatomy.” *WebMD*. <https://www.webmd.com/skin-problems-and-treatments/picture-of-the-skin> (February 27, 2021).
- Tomita, Koichi, Nishibayashi Akimitsu, Yano Kenji, and Ko Hosokawa. 2020. “Differentiated Adipose-Derived Stem Cells Promote Reinnervation of Rat Skin Flaps.” *Nature* 388: 539–47.
- Vaux, J. J. et al. 2016. “Morphometrics of the Human Thumb Metacarpal Bone: Interest for Developing an Osseointegrated Prosthesis.” *Surgical and Radiologic Anatomy* 38(1): 127–33.
- Vig, Komal et al. 2017. “Advances in Skin Regeneration Using Tissue Engineering.”

International Journal of Molecular Sciences 18(4).

Webster, H. R., and D. W. Robinson. 1995. "The Radial Forearm Flap without Fascia and Other Refinements." *European Journal of Plastic Surgery* 18(1): 11–13.

Zeng, Li et al. "A Noninvasive Functional Evaluation Following Peripheral Nerve Repair with Electromyography in a Rat Model."